A&A 596, A108 (2016)
DOI: 10.1051/0004-6361/201628897

Astronomy & Astrophysics

Planck intermediate results

XLVII. *Planck* constraints on reionization history

Planck Collaboration: R. Adam[67], N. Aghanim[53], M. Ashdown[63,7], J. Aumont[53], C. Baccigalupi[75], M. Ballardini[29,45,48], A. J. Banday[85,10], R. B. Barreiro[58], N. Bartolo[28,59], S. Basak[75], R. Battye[61], K. Benabed[54,84], J.-P. Bernard[85,10], M. Bersanelli[32,46], P. Bielewicz[72,10,75], J. J. Bock[60,11], A. Bonaldi[61], L. Bonavera[16], J. R. Bond[9], J. Borrill[12,81], F. R. Bouchet[54,79], F. Boulanger[53], M. Bucher[1], C. Burigana[45,30,48], E. Calabrese[82], J.-F. Cardoso[66,1,54], J. Carron[21], H. C. Chiang[23,8], L. P. L. Colombo[19,60], C. Combet[67], B. Comis[67], F. Couchot[64], A. Coulais[65], B. P. Crill[60,11], A. Curto[58,7,63], F. Cuttaia[45], R. J. Davis[61], P. de Bernardis[31], A. de Rosa[45], G. de Zotti[42,75], J. Delabrouille[1], E. Di Valentino[54,79], C. Dickinson[61], J. M. Diego[58], O. Doré[60,11], M. Douspis[53], A. Ducout[54,52], X. Dupac[36], F. Elsner[20,54,84], T. A. Enßlin[70], H. K. Eriksen[56], E. Falgarone[65], Y. Fantaye[34,3], F. Finelli[45,48], F. Forastieri[30,49], M. Frailis[44], A. A. Fraisse[23], E. Franceschi[45], A. Frolov[78], S. Galeotta[44], S. Galli[62], K. Ganga[1], R. T. Génova-Santos[57,15], M. Gerbino[83,74,31], T. Ghosh[53], J. González-Nuevo[16,58], K. M. Górski[60,87], A. Gruppuso[45,48], J. E. Gudmundsson[83,74,23], F. K. Hansen[56], G. Helou[11], S. Henrot-Versillé[64], D. Herranz[58], E. Hivon[54,84], Z. Huang[9], S. Ilić[85,10,6], A. H. Jaffe[52], W. C. Jones[23], E. Keihänen[22], R. Keskitalo[12], T. S. Kisner[69], L. Knox[25], N. Krachmalnicoff[32], M. Kunz[14,53,3], H. Kurki-Suonio[22,41], G. Lagache[5,53], A. Lähteenmäki[2,41], J.-M. Lamarre[65], M. Langer[53], A. Lasenby[7,63], M. Lattanzi[30,49], C. R. Lawrence[60], M. Le Jeune[1], F. Levrier[65], A. Lewis[21], M. Liguori[28,59], P. B. Lilje[56], M. López-Caniego[36], Y.-Z. Ma[61,76], J. F. Macías-Pérez[67], G. Maggio[44], A. Mangilli[53,64], M. Maris[44], P. G. Martin[9], E. Martínez-González[58], S. Matarrese[28,59,38], N. Mauri[48], J. D. McEwen[71], P. R. Meinhold[26], A. Melchiorri[31,50], A. Mennella[32,46], M. Migliaccio[55,63], M.-A. Miville-Deschênes[53,9], D. Molinari[30,45,49], A. Moneti[54], L. Montier[85,10], G. Morgante[45], A. Moss[77], P. Naselsky[73,35], P. Natoli[30,4,49], C. A. Oxborrow[13], L. Pagano[31,50], D. Paoletti[45,48], B. Partridge[40], G. Patanchon[1], L. Patrizii[48], O. Perdereau[64], L. Perotto[67], V. Pettorino[39], F. Piacentini[31], S. Plaszczynski[64], L. Polastri[30,49], G. Polenta[4,43], J.-L. Puget[53], J. P. Rachen[17,70], B. Racine[56], M. Reinecke[70], M. Remazeilles[61,53,1], A. Renzi[34,51], G. Rocha[60,11], M. Rossetti[32,46], G. Roudier[1,65,60], J. A. Rubiño-Martín[57,15], B. Ruiz-Granados[86], L. Salvati[31], M. Sandri[45], M. Savelainen[22,41], D. Scott[18], G. Sirri[48], R. Sunyaev[70,80], A.-S. Suur-Uski[22,41], J. A. Tauber[37], M. Tenti[47], L. Toffolatti[16,58,45], M. Tomasi[32,46], M. Tristram[64,⋆], T. Trombetti[45,30], J. Valiviita[22,41], F. Van Tent[68], P. Vielva[58], F. Villa[45], N. Vittorio[33], B. D. Wandelt[54,84,27], I. K. Wehus[60,56], M. White[24], A. Zacchei[44], and A. Zonca[26]

(Affiliations can be found after the references)

Received 11 May 2016 / Accepted 23 July 2016

ABSTRACT

We investigate constraints on cosmic reionization extracted from the *Planck* cosmic microwave background (CMB) data. We combine the *Planck* CMB anisotropy data in temperature with the low-multipole polarization data to fit ΛCDM models with various parameterizations of the reionization history. We obtain a Thomson optical depth $\tau = 0.058 \pm 0.012$ for the commonly adopted instantaneous reionization model. This confirms, with data solely from CMB anisotropies, the low value suggested by combining *Planck* 2015 results with other data sets, and also reduces the uncertainties. We reconstruct the history of the ionization fraction using either a symmetric or an asymmetric model for the transition between the neutral and ionized phases. To determine better constraints on the duration of the reionization process, we also make use of measurements of the amplitude of the kinetic Sunyaev-Zeldovich (kSZ) effect using additional information from the high-resolution Atacama Cosmology Telescope and South Pole Telescope experiments. The average redshift at which reionization occurs is found to lie between $z = 7.8$ and 8.8, depending on the model of reionization adopted. Using kSZ constraints and a redshift-symmetric reionization model, we find an upper limit to the width of the reionization period of $\Delta z < 2.8$. In all cases, we find that the Universe is ionized at less than the 10% level at redshifts above $z \simeq 10$. This suggests that an early onset of reionization is strongly disfavoured by the *Planck* data. We show that this result also reduces the tension between CMB-based analyses and constraints from other astrophysical sources.

Key words. cosmic background radiation – dark ages, reionization, first stars – polarization

1. Introduction

The process of cosmological recombination happened around redshift $z \simeq 1100$, after which the ionized fraction fell precipitously (Peebles 1968; Zel'dovich et al. 1969; Seager et al. 2000) and the Universe became mostly neutral. However, observations of the Gunn-Peterson effect (Gunn & Peterson 1965) in quasar spectra (Becker et al. 2001, 2015; Fan et al. 2006b; Venemans et al. 2013) indicate that intergalactic gas had become almost fully reionized by redshift $z \simeq 6$. Reionization is thus the second major change in the ionization state of hydrogen in the Universe. Details of the transition from the neutral to ionized Universe are still the subject of intense investigations (for a recent review, see the book by Mesinger 2016). In the currently conventional picture, early galaxies reionize hydrogen progressively throughout the entire Universe between $z \simeq 12$ and $z \simeq 6$, while quasars take over to reionize helium from $z \simeq 6$ to $\simeq 2$. But many questions remain. When did the epoch of reionization (EoR) start, and how long did it last? Are early galaxies enough to reionize the entire Universe or is another source required? We try to shed light on these questions using the traces left by the EoR in the cosmic microwave background (CMB) anisotropies.

⋆ Corresponding authors:
M. Tristram, e-mail: tristram@lal.in2p3.fr;
M. Douspis, e-mail: marian.douspis@ias.u-psud.fr

The CMB is affected by the total column density of free electrons along each line of sight, parameterized by its Thomson scattering optical depth τ. This is one of the six parameters of the baseline Λ cold dark matter (CDM) cosmological model and is the key measurement for constraining reionization. Large-scale anisotropies in polarization are particularly sensitive to the value of τ. The WMAP mission was the first to extract a τ measurement through the correlation between the temperature field and the E-mode polarization (i.e., the TE power spectrum) over a large fraction of the sky. This measurement is very demanding, since the expected level of the E-mode polarization power spectrum at low multipoles ($\ell < 10$) is only a few times $10^{-2}\,\mu\mathrm{K}^2$, lower by more than two orders of magnitude than the level of the temperature anisotropy power spectrum. For such weak signals the difficulty is not only to have enough detector sensitivity, but also to reduce and control both instrumental systematic effects and foreground residuals to a very low level. This difficulty is illustrated by the improvements over time in the WMAP-derived τ estimates. The 1-yr results gave a value of $\tau = 0.17 \pm 0.04$, based on the temperature-polarization TE cross-power spectrum (Kogut et al. 2003). In the 3-yr release, this was revised down to 0.10 ± 0.03 using E-modes alone, whereas the combined TT, TE, and EE power spectra gave 0.09 ± 0.03 (Page et al. 2007). Error bars improved in further WMAP analyses, ending up with 0.089 ± 0.014 after the 9-yr release (see Dunkley et al. 2009; Komatsu et al. 2011; Hinshaw et al. 2013). In 2013, the first *Planck* satellite[1] cosmological results were based on *Planck* temperature power spectra combined with the polarized WMAP data and gave the same value $\tau = 0.089 \pm 0.014$ (Planck Collaboration XVI 2014). However, using a preliminary version of the *Planck* 353 GHz polarization maps to clean the dust emission (in place of the WMAP dust model), the optical depth was reduced by approximately 1σ to $\tau = 0.075 \pm 0.013$ (Planck Collaboration XV 2014).

In the 2015 Planck analysis (Planck Collaboration XIII 2016), the Low Frequency Instrument (LFI) low-resolution maps polarization at 70 GHz were used. Foreground cleaning was performed using the LFI 30 GHz and High Frequency Instrument (HFI) 353 GHz maps, operating effectively as polarized synchrotron and dust templates, respectively. The optical depth was found to be $\tau = 0.078 \pm 0.019$, and this decreased to 0.066 ± 0.016 when adding CMB lensing data. This value is also in agreement with the constraints from the combination "PlanckTT+lensing+BAO", yielding $\tau = 0.067 \pm 0.016$, which uses no information from low-ℓ polarization.

In this paper and its companion (Planck Collaboration Int. XLVI 2016), we derive the first estimate of τ from the *Planck*-HFI polarization data at large scales. For the astrophysical interpretation, the power spectra are estimated using a PCL estimate which is more conservative. Indeed, it gives a slightly larger distribution on τ than the QML estimator used in Planck Collaboration Int. XLVI (2016) but is less sensitive to the limited number of simulations available for the analysis. Using only E-mode polarization, the *Planck* `lollipop` likelihood gives $\tau = 0.053^{+0.014}_{-0.016}$ for a standard instantaneous reionization model, when all other ΛCDM parameters are fixed to their *Planck*-2015 best-fit values. We show that in combination with the *Planck* temperature data the error bars are improved and we find $\tau = 0.058 \pm 0.012$.

In the ΛCDM model, improved accuracy on the reionization optical depth helps to reduce the degeneracies with other parameters. In particular, the measurement of τ reduces the correlation with the normalization of the initial power spectrum A_s and its spectral index n_s. In addition to this τ is a particularly important source of information for constraining the history of reionization, which is the main subject of this paper. When combined with direct probes at low redshift, a better knowledge of the value of the CMB optical depth parameter may help to characterize the duration of the EoR, and thus tell us when it started.

In addition to the effect of reionization on the polarized large-scale CMB anisotropies, reionization generates CMB temperature anisotropies through the kinetic Sunyaev-Zeldovich (kSZ) effect (Sunyaev & Zeldovich 1980), caused by the Doppler shift of photons scattering off electrons moving with bulk velocities. Simulations have shown that early homogeneous and patchy reionization scenarious differently affect the shape of the kSZ power spectrum, allowing us to place constraints on the reionization history (e.g., McQuinn et al. 2005; Aghanim et al. 2008). Zahn et al. (2012) derived the first constraints on the epoch of reionization from the combination of kSZ and low-ℓ CMB polarization, specifically using the low-ℓ polarization power spectrum from WMAP and the very high multipoles of the temperature angular power spectrum from the South Pole Telescope (SPT, Reichardt et al. 2012). However one should keep in mind that kSZ signal is complicated to predict and depends on detailed astrophysics which makes the constraints on reionization difficult to interpret (Mesinger et al. 2012).

In this paper, we investigate constraints on the epoch of reionization coming from *Planck*. Section 2 first briefly describes the pre-2016 data and likelihood used in this paper, which are presented in detail in Planck Collaboration Int. XLVI (2016). In Sect. 3 we then present the parameterizations we adopt for the ionization fraction, describing the reionization history as a function of redshift. In Sect. 4, we show the results obtained from the CMB observables (i.e., the optical depth τ and the amplitude of the kSZ effect) in the case of "instantaneous" reionization. Section 5 presents results based on the CMB measurements by considering different models for the ionization history. In particular, we derive limits on the reionization redshift and duration. Finally, in Sect. 6, we derive the ionization fraction as a function of redshift and discuss how our results relate to other astrophysical constraints.

2. Data and likelihood

2.1. Data

The present analysis is based on the pre-2016 full mission intensity and polarization *Planck*-HFI maps at 100 and 143 GHz. The data processing and the beam description are the same as in the *Planck* 2015 release and have been detailed in Planck Collaboration VII (2016). *Planck*-HFI polarization maps are constructed from the combination of polarized detectors that have fixed polarization direction. The *Planck* scanning strategy produces a relatively low level of polarization angle measurement redundancy on the sky, resulting in a high level of I-Q-U mixing, as shown in Planck Collaboration VIII (2016). As a consequence, any instrumental mismatch between detectors from the same frequency channel produces leakage from intensity to polarization. This temperature-to-polarization leakage was at one point the main systematic effect present in the

[1] *Planck* (`http://www.esa.int/Planck`) is a project of the European Space Agency (ESA) with instruments provided by two scientific consortia funded by ESA member states and led by Principal Investigators from France and Italy, telescope reflectors provided through a collaboration between ESA and a scientific consortium led and funded by Denmark, and additional contributions from NASA (USA).

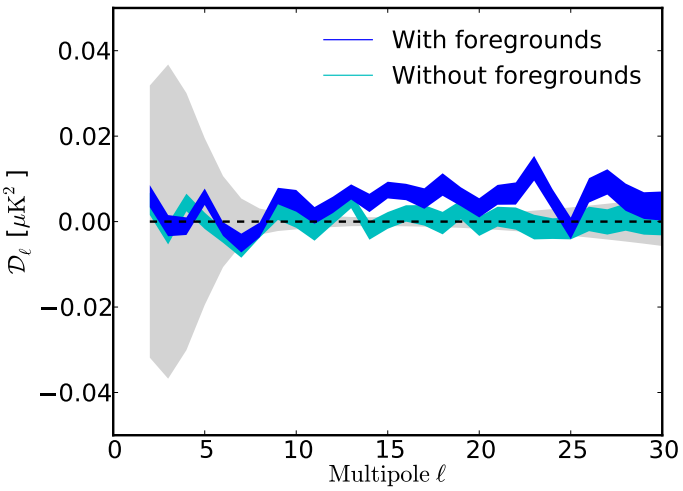

Fig. 1. Bias in the 100 × 143 cross-power spectrum computed from simulations, including instrumental noise and systematic effects, with or without foregrounds (dark blue and light blue), compared to the cosmic variance level (in grey).

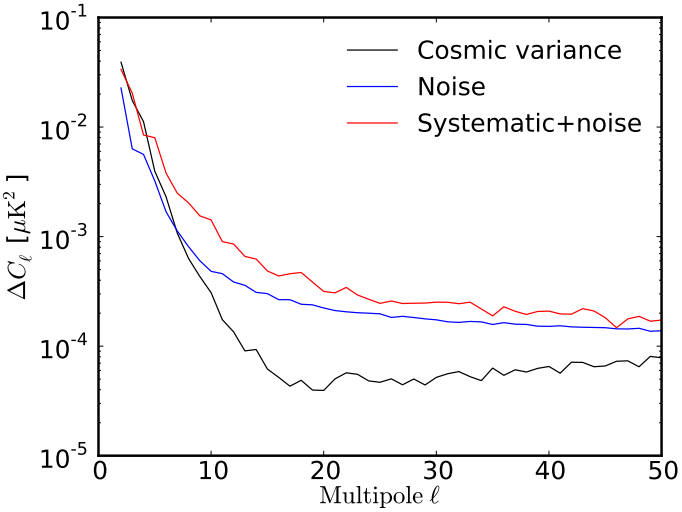

Fig. 2. Variance of the 100 × 143 *EE* cross-power spectrum for simulations, including instrumental noise and noise plus systematic effects, compared to cosmic variance.

Planck-HFI data, and prevented robust low-ℓ polarization measurements from being included in the previous *Planck* data releases.

The maps that we use here differ in some respects from those data released in 2015. The updated mapmaking procedure, presented in Planck Collaboration Int. XLVI (2016), now allows for a significant reduction of the systematic effects in the maps. In particular, the relative calibration within a channel is now accurate to better than 0.001%, which ensures a very low level of gain-mismatch between detectors. The major systematic effect that remains in the pre-2016 maps is due to imperfections of the correction for nonlinearity in the analogue-to-digital converters (ADCs) but produces very low level of residuals in the maps. In addition to the 100 GHz and 143 GHz maps, we also make use of 30 GHz LFI data (Planck Collaboration II 2016) and 353 GHz HFI data to remove polarized foregrounds.

Using the pre-2016 end-to-end simulations, we show that the power spectrum bias induced by the remaining nonlinearities is very small and properly accounted for in the likelihood. Figure 1 shows the bias (in the quantity $\mathcal{D}_\ell \equiv \ell(\ell+1)C_\ell/2\pi$, where C_ℓ is the conventional power spectrum) computed as the mean of the *EE* cross-power spectra from simulated maps, including realistic noise and systematic effects without and with Galactic foregrounds. In the latter case, the foregrounds are removed for each simulation using the 30 GHz and 353 GHz maps as templates for synchrotron and dust, respectively. The resulting bias in the *EE* 100 × 143 cross-power spectrum can be used to correct the measured cross-spectrum, but in fact has very little impact on the likelihood.

Furthermore, we use end-to-end simulations to propagate the systematic uncertainties to the cross-power spectra and all the way to the cosmological parameters. Figure 2 shows the impact on the variance due to the inclusion of the main ADC nonlinearity systematic effect, compared to realistic noise and cosmic variance. The resulting C_ℓ covariance matrix is estimated from these Monte Carlos. In the presence of such systematic effects, the variance of the C_ℓ is shown to be higher by roughly a factor of 2 compared to the pure noise case.

Polarized foregrounds at *Planck*-HFI frequencies are essentially dominated by Galactic dust emission, but also include a small contribution from synchrotron emission. We use the 353 GHz and 30 GHz *Planck* maps as templates to subtract dust and synchrotron, respectively, using a single coefficient for each component over 95% of the sky (see Planck Collaboration IX 2016; Planck Collaboration X 2016). However, foreground residuals in the maps are still dominant over the CMB polarized signal near the Galactic plane. We therefore apply a very conservative mask, based on the amplitude of the polarized dust emission, which retains 50% of the sky for the cosmological analysis. Outside this mask, the foreground residuals are found to be lower than 0.3 and 0.4 μK in Q and U Stokes polarization maps at 100 and 143 GHz, respectively. We have checked that our results are very stable when using a larger sky fraction of 60%.

In this paper, we also make use of the constraints derived from the observation of the Gunn-Peterson effect on high-redshift quasars. As suggested by Fan et al. (2006a), these measurements show that the Universe was almost fully reionized at redshift $z \simeq 6$. We later discuss the results obtained with and without imposing a prior on the redshift of the end of reionization.

2.2. Likelihood

For temperature anisotropies, we use the combined *Planck* likelihood (hereafter "PlanckTT"), which includes the *TT* power spectrum likelihood at multipoles $\ell > 30$ (using the `Plik` code) and the low-ℓ temperature-only likelihood based on the CMB map recovered from the component-separation procedure (specifically `Commander`) described in detail in Planck Collaboration XI (2016).

For polarization, we use the *Planck* low-ℓ *EE* polarization likelihood (hereafter `lollipop`), a cross-spectra-based likelihood approach described in detail in Mangilli et al. (2015) and applied to *Planck* data as discussed here in Appendix A. The multipole range used is $\ell = 4$–20. Cross-spectra are estimated using the pseudo-C_ℓ estimator `Xpol` (a generalization to polarization of the algorithm presented in Tristram et al. 2005). For a full-sky analysis, the statistics of the reconstructed C_ℓ are given by a χ^2 distribution that is uncorrelated between multipoles. For a cut-sky analysis, the distribution is more complex and

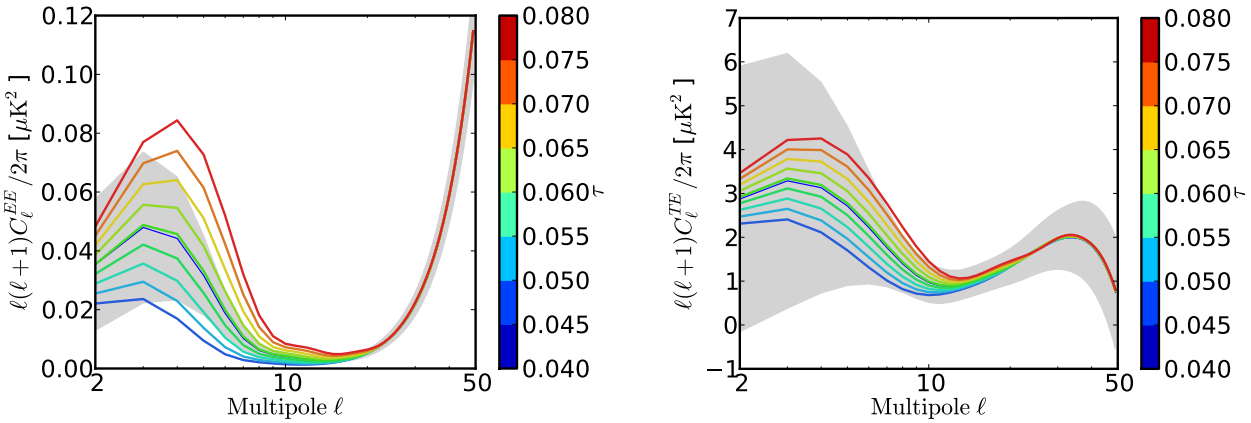

Fig. 3. EE and TE power spectra for various τ values ranging from 0.04 to 0.08. The ionization fraction is modelled using a redshift-symmetric tanh function with $\delta z = 0.5$. Grey bands represent the cosmic variance (full-sky) associated with the $\tau = 0.06$ model.

includes ℓ-to-ℓ correlations. Hamimeche & Lewis (2008) proposed an approximation of the likelihood for cut-sky auto-power spectra that was adapted by Mangilli et al. (2015) to be suitable for cross-spectra. Cross-spectra between independent data sets show common sky signal, but are not biased by the noise because this should be uncorrelated. This approximation assumes that any systematic residuals are *not* correlated between the different data sets; We have shown using realistic simulations (including *Planck*-HFI noise characteristics and systematic effect residuals), that the bias in the cross-spectra is very small and can be corrected for at the power-spectrum level. Nevertheless, we choose to remove the first two multipoles ($\ell = 2$ and $\ell = 3$), since they may still be partially contaminated by systematics. Using those simulations, we derive the C_ℓ covariance matrix used in the likelihood, which propagates both the noise and the systematic uncertainties. For the astrophysical interpretation, the power-spectra are estimated with a PCL estimate which is more conservative. Indeed, it gives a slightly larger distribution on τ than a QML estimator but is less sensitive to the limited number of simulations available for the analysis.

With *Planck* sensitivity in polarization, the results from the low-ℓ EE power spectrum dominate the constraints compared to the TE power spectrum, as can be seen in Fig. 3. This is because of the relatively larger cosmic variance for TE (arising from the temperature term) and the intrinsically weaker dependence on τ ($\propto\tau$ compared with τ^2 for EE), as well as the fact that there is only partial correlation between T and E. As a consequence, we do not consider the TE data in this analysis. Furthermore, we do not make use of the high-ℓ likelihoods in EE and TE from *Planck*, since they do not carry additional information on reionization parameters.

Planck temperature observations are complemented at smaller angular scales by measurements from the ground-based Atacama Cosmology Telescope (ACT) and South Pole Telescope (SPT). As explained in Planck Collaboration XI (2016), the high-ℓ likelihood (hereafter VHL) includes ACT power spectra at 148 and 218 GHz (Das et al. 2014), with a revised binning (described in Calabrese et al. 2013) and final beam estimates (Hasselfield et al. 2013), together with SPT measurements in the range $2000 < \ell < 13\,000$ from the 2540 deg^2 SPT-SZ survey at 95, 150, and 220 GHz (George et al. 2015). To assess the consistency between these data sets, we extend the *Planck* foreground models up to $\ell = 13\,000$, with additional nuisance parameters for ACT and SPT (as described in Planck Collaboration XIII 2016). We use the same models for cosmic infrared background (CIB) fluctuations, the thermal SZ (tSZ) effect, kSZ effect, and CIB × tSZ components. The kSZ template used in the *Planck* 2015 results assumed homogeneous reionization. In order to investigate inhomogeneous reionization, we have modified the kSZ template when necessary, as discussed in Sect. 4.2.

We use the CMB lensing likelihood (Planck Collaboration XV 2016) in addition to the CMB anisotropy likelihood. The lensing information can be used to break the degeneracy between the normalization of the initial power spectrum A_s and τ (as discussed in Planck Collaboration XIII 2016). Despite this potential for improvement, we show in Sect. 4.1 that *Planck*'s low-ℓ polarization signal-to-noise ratio is sufficiently high that the lensing does not bring much additional information for the reionization constraints.

The *Planck* reference cosmology used in this paper corresponds to the PlanckTT+lowP+lensing best fit, as described in Table 4, Col. 2 of Planck Collaboration XIII (2016), namely $\Omega_b h^2 = 0.02226$, $\Omega_c h^2 = 0.1197$, $\Omega_m = 0.308$, $n_s = 0.9677$, $H_0 = 67.81\,\mathrm{km\,s^{-1}\,Mpc^{-1}}$, for which $Y_P = 0.2453$. This best-fit model comes from the combination of three *Planck* likelihoods: the temperature power spectrum likelihood at high ℓ; the "lowP" temperature+polarization likelihood, based on the foreground-cleaned LFI 70 GHz polarization maps, together with the temperature map from the `Commander` component-separation algorithm; and the power spectrum of the lensing potential as measured by *Planck*.

3. Parametrization of reionization history

The epoch of reionization (EoR) is the period during which the cosmic gas transformed from a neutral to ionized state at the onset of the first sources. Details of the transition are thus strongly connected to many fundamental questions in cosmology, such as what were the properties of the first galaxies and the first (mini-)quasars, how did the formation of very metal-poor stars proceed, etc. We certainly know that, at some point, luminous sources started emitting ultraviolet radiation that reionized the neutral regions around them. After a sufficient number of ionizing sources had formed, the average ionized fraction of the gas in the Universe rapidly increased until hydrogen became fully ionized. Empirical, analytic, and numerical models of the reionization process have highlighted many pieces of the essential physics that led to the birth to the ionized intergalactic medium (IGM) at late times (Couchman & Rees 1986; Miralda-Escude & Ostriker 1990;

Meiksin & Madau 1993; Aghanim et al. 1996; Gruzinov & Hu 1998; Madau et al. 1999; Gnedin 2000; Barkana & Loeb 2001; Ciardi et al. 2003; Furlanetto et al. 2004; Pritchard et al. 2010; Pandolfi et al. 2011; Mitra et al. 2011; Iliev et al. 2014). Such studies provide predictions on the various reionization observables, including those associated with the CMB.

The most common physical quantity used to characterize reionization is the Thomson scattering optical depth defined as

$$\tau(z) = \int_{t(z)}^{t_0} n_e \sigma_T \, c \mathrm{d}t', \tag{1}$$

where n_e is the number density of free electrons at time t', σ_T is the Thomson scattering cross-section, t_0 is the time today, $t(z)$ is the time at redshift z, and we can use the Friedmann equation to convert dt to dz. The reionization history is conveniently expressed in terms of the ionized fraction $x_e(z) \equiv n_e(z)/n_H(z)$ where $n_H(z)$ is the hydrogen number density. In practice, the CMB is sensitive to the average over all sky directions of $x_e(1+\delta_b)$ (where δ_b denotes the baryon overdensity). The IGM is likely to be very inhomogeneous during reionization process, with ionized bubbles embedded in neutral surroundings, which would impact the relation between the optical depth and the reionisation parameters (see Liu et al. 2016) at a level which is neglected in this paper.

In this study, we define the redshift of reionization, $z_{re} \equiv z_{50\%}$, as the redshift at which $x_e = 0.5 \times f$. Here the normalization, $f = 1 + f_{He} = 1 + n_{He}/n_H$, takes into account electrons injected into the IGM by the first ionization of helium (corresponding to 25 eV), which is assumed to happen roughly at the same time as hydrogen reionization. We define the beginning and the end of the EoR by the redshifts $z_{beg} \equiv z_{10\%}$ and $z_{end} \equiv z_{99\%}$ at which $x_e = 0.1 \times f$ and $0.99 \times f$, respectively. The duration of the EoR is then defined as $\Delta z = z_{10\%} - z_{99\%}$[2]. Moreover, to ensure that the Universe is fully reionized at low redshift, we impose the condition that the EoR is completed before the second helium reionization phase (corresponding to 54 eV), noting that it is commonly assumed that quasars are necessary to produce the hard photons needed to ionize helium. To be explicit about how we treat the lowest redshifts we assume that the full reionization of helium happens fairly sharply at $z_{He} = 3.5$ (Becker et al. 2011), following a transition of hyperbolic tangent shape with width $\delta z = 0.5$. While there is still some debate on whether helium reionization could be inhomogeneous and extended (and thus have an early start, Worseck et al. 2014), we have checked that varying the helium reionization redshift between 2.5 and 4.5 changes the total optical depth by less than 1%.

The simplest and most widely-used parameterizations describes the EoR as a step-like transition between an essentially vanishing ionized fraction[3] x_e at early times, to a value of unity at low redshifts. When calculating the effect on anisotropies it is necessary to give a non-zero width to the transition, and it can be modelled using a tanh function (Lewis 2008):

$$x_e(z) = \frac{f}{2}\left[1 + \tanh\left(\frac{y - y_{re}}{\delta y}\right)\right], \tag{2}$$

where $y = (1+z)^{3/2}$ and $\delta y = \frac{3}{2}(1+z)^{1/2}\delta z$. The key parameters are thus z_{re}, which measures the redshift at which the ionized fraction reaches half its maximum and a width δz. The tanh parameterization of the EoR transition allows us to compute the optical depth of Eq. (1) for a one-stage almost redshift-symmetric[4] reionization transition, where the redshift interval between the onset of the reionization process and its half completion is (by construction) equal to the interval between half completion and full completion. In this parameterization, the optical depth is mainly determined by z_{re} and almost degenerate with the width δz. This is the model used in the *Planck* 2013 and 2015 cosmological papers, for which we have fixed $\delta z = 0.5$ (corresponding to $\Delta z = 1.73$). In this case, we usually talk about "instantaneous" reionization.

A redshift-asymmetric parameterization is a better, more flexible description of numerical simulations of the reionization process (e.g., Ahn et al. 2012; Park et al. 2013; Douspis et al. 2015). A function with this behaviour is also suggested by the constraints from ionizing background measurements of star-forming galaxies and from low-redshift line-of-sight probes such as quasars, Lyman-α emitters, or γ-ray bursts (Faisst et al. 2014; Chornock et al. 2014; Ishigaki et al. 2015; Robertson et al. 2015; Bouwens et al. 2015). The two simplest choices of redshift-asymmetric parameterizations are polynomial or exponential functions of redshift (Douspis et al. 2015). These two parameterizations are in fact very similar, and we adopt here a power law defined by two parameters: the redshift at which reionization ends (z_{end}); and the exponent α. Specifically we have

$$x_e(z) = \begin{cases} f & \text{for } z < z_{end}, \\ f\left(\frac{z_{early} - z}{z_{early} - z_{end}}\right)^{\alpha} & \text{for } z > z_{end}. \end{cases} \tag{3}$$

In the following, we fix $z_{early} = 20$, the redshift around which the first emitting sources form, and at which we smoothly match $x_e(z)$ to the ionized fraction left over from recombination. We checked that our results are not sensitive to the precise value of z_{early}, as long as it is not dramatically different.

Non-parametric reconstructions of the ionization fraction have also been proposed to probe the reionization history. Such methods are based on exploring reionization parameters in bins of redshift (Lewis et al. 2006). They should be particularly useful for investigating exotic reionization histories, e.g., double reionization (Cen 2003). However, the CMB large-scale ($\ell \lesssim 10$) polarization anisotropies are mainly sensitive to the overall value of the optical depth, which determines the amplitude of the reionization bump in the EE power spectrum (see Fig. 3). We have estimated the impact on C_ℓ^{EE} for the two different models (tanh and power law) having the same $\tau = 0.06$ and found differences of less than 4% for $\ell < 10$. Even for a double reionization model, Fig. 4 shows that the impact on C_ℓ^{EE} is quite weak, given the actual measured value of τ, and cannot be distinguished relative to the cosmic variance spread (i.e., even for a full-sky experiment). We also checked that *Planck* data do not allow for model-independent reconstruction of x_e in redshift bins. Principal component analysis has been proposed as an explicit approach to try to capture the details of the reionization history in a small set of parameters (Hu & Holder 2003; Mortonson & Hu 2008). Although these methods are generally considered to be non-parametric, they are in fact based on a description of $x_e(z)$

[2] The reason this is not defined symmetrically is that in practice we have tighter constraints on the end of reionization than on the beginning.

[3] The ionized fraction is actually matched to the relic free electron density from recombination, calculated using `recfast` Seager et al. (2000).

[4] For convenience, we refer to this parameterization as "redshift symmetric" in the rest of the paper, even although it is actually symmetric in y rather than z. The asymmetry is maximum in the instantaneous case, but the difference in x_e values around, for example, $z_{re} = 8 \pm 1$, is less than 1%.

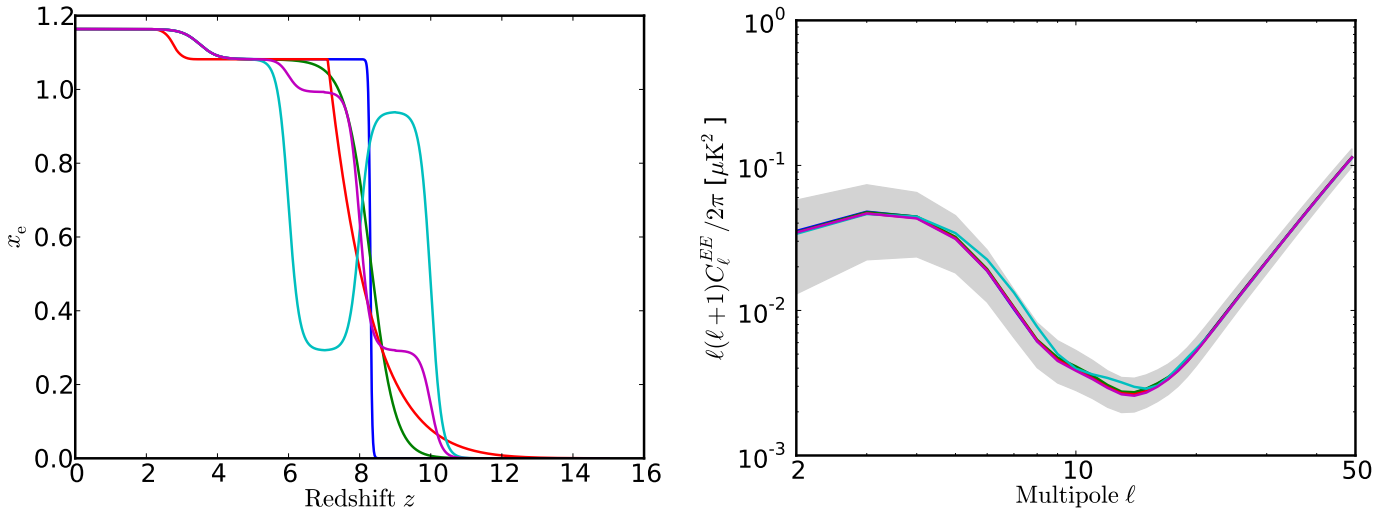

Fig. 4. *Left*: evolution of the ionization fraction for several functions, all having the same optical depth, $\tau = 0.06$: green and blue are for redshift-symmetric instantaneous ($\delta z = 0.05$) and extended reionization ($\delta z = 0.7$), respectively; red is an example of a redshift-asymmetric parameterization; and light blue and magenta are examples of an ionization fraction defined in redshift bins, with two bins inverted between these two examples. *Right*: corresponding EE power spectra with cosmic variance in grey. All models have the same optical depth $\tau = 0.06$ and are essentially indistinguishable at the reionization bump scale.

in bins of redshift, expanded around a given fiducial model for C_ℓ^{EE}. Moreover, the potential bias on the τ measurement when analysing a more complex reionization history using a simple sharp transition model (Holder et al. 2003; Colombo & Pierpaoli 2009) is considerably reduced for the (lower) τ values as suggested by the *Planck* results. Consequently, we do not consider the non-parametric approach further.

4. Measuring reionization observables

Reionization leaves imprints in the CMB power spectra, both in polarization at very large scales and in intensity via the suppression of TT power at higher ℓ. Reionization also affects the kSZ effect, due to the re-scattering of photons off newly liberated electrons. We sample from the space of possible parameters with MCMC exploration using CAMEL[5]. This uses an adaptative-Metropolis algorithm to generate chains of samples for a set of parameters.

4.1. Large-scale CMB polarization

Thomson scattering between the CMB photons and free electrons generates linear polarization from the quadrupole moment of the CMB radiation field at the scattering epoch. This occurs at recombination and also during the epoch of reionization. Re-scattering of the CMB photons at reionization generates an additional polarization anisotropy at large angular scales, because the horizon size at this epoch subtends a much larger angular size. The multipole location of this additional anisotropy (essentially a bump) in the EE and TE angular power spectra relates to the horizon size at the new "last-rescattering surface" and thus depends on the redshift of reionization. The height of the bump is a function of the optical depth or, in other words, of the history of the reionization process. Such a signature (i.e., a polarization bump at large scales) was first observed by WMAP, initially in the TE angular power spectrum (Kogut et al. 2003), and later in combination with all power spectra (Hinshaw et al. 2013).

In Fig. 3 we show for the "instantaneous" reionization case (specifically the redshift-symmetric parameterization with $\delta z = 0.5$) power spectra for the E-mode polarization power spectrum C_ℓ^{EE} and the temperature-polarization cross-power spectrum C_ℓ^{TE}. The curves are computed with the `CLASS` Boltzmann solver (Lesgourgues 2011) using τ values ranging from 0.04 to 0.08. For the range of optical depth considered here and given the amount of cosmic variance, the TE spectrum has only a marginal sensitivity to τ, while in EE the ability to distinguish different values of τ is considerably stronger.

In Fig. 4 (left panel), the evolution of the ionized fraction x_e during the EoR is shown for five different parameterizations of the reionization history, all yielding the same optical depth $\tau = 0.06$. Despite the differences in the evolution of the ionization fraction, the associated C_ℓ^{EE} curves (Fig. 4, right panel) are almost indistinguishable. This illustrates that while CMB large-scale anisotropies in polarization are only weakly sensitive to the details of the reionization history, they can nevertheless be used to measure the reionization optical depth, which is directly related to the amplitude of the low-ℓ bump in the E-mode power spectrum.

We use the *Planck* data to provide constraints on the Thomson scattering optical depth for "instantaneous" reionization. Figure 5 shows the posterior distributions for τ obtained with the different data sets described in Sect. 2 and compared to the 2015 PlanckTT+lowP results (Planck Collaboration XIII 2016). We show the posterior distribution for the low-ℓ *Planck* polarized likelihood (`lollipop`) and in combination with the high-ℓ *Planck* likelihood in temperature (PlanckTT). We also consider the effect of adding the SPT and ACT likelihoods (VHL) and the *Planck* lensing likelihood, as described in Planck Collaboration XV (2016).

The different data sets show compatible constraints on the optical depth τ. The comparison between posteriors indicates that the optical depth measurement is driven by the low-ℓ likelihood in polarization (i.e., `lollipop`). The *Planck* constraints on τ for a ΛCDM model when considering the standard "instantaneous" reionization assumption (symmetric model with fixed

[5] Available at `camel.in2p3.fr`

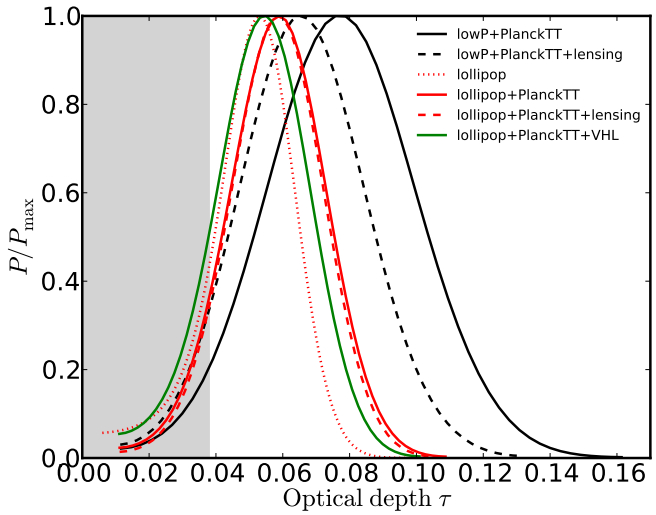

Fig. 5. Posterior distribution for τ from the various combinations of *Planck* data. The grey band shows the lower limit on τ from the Gunn-Peterson effect.

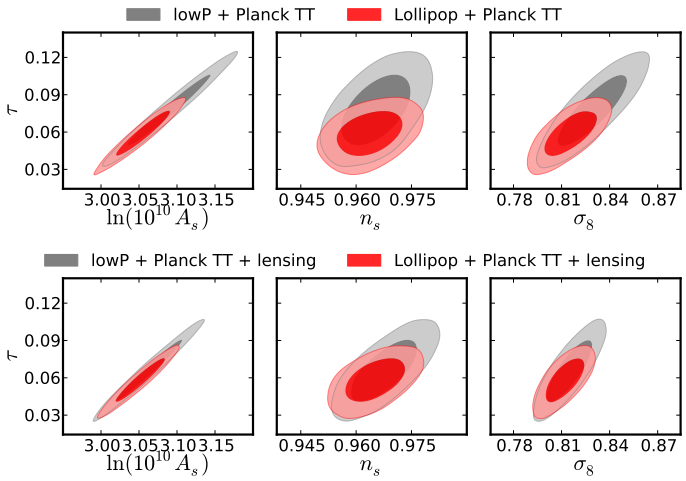

Fig. 6. Constraints on τ, $A_{\rm s}$, $n_{\rm s}$, and σ_8 for the ΛCDM cosmology from PlanckTT, showing the impact of replacing the lowP likelihood from *Planck* 2015 release with the new `lollipop` likelihood. *The top panels* show results without lensing, while *the bottom panels* are with lensing.

$\delta z = 0.5$), for the various data combinations are:

$$\tau = 0.053^{+0.014}_{-0.016}, \quad \texttt{lollipop}^{6}; \tag{4}$$

$$\tau = 0.058^{+0.012}_{-0.012}, \quad \texttt{lollipop+PlanckTT}; \tag{5}$$

$$\tau = 0.058^{+0.011}_{-0.012}, \quad \texttt{lollipop+PlanckTT+lensing}; \tag{6}$$

$$\tau = 0.054^{+0.012}_{-0.013}, \quad \texttt{lollipop+PlanckTT+VHL}. \tag{7}$$

We can see an improvement of the posterior width when adding temperature anisotropy data to the `lollipop` likelihood. This comes from the fact that the temperature anisotropies help to fix other ΛCDM parameters, in particular the normalization of the initial power spectrum $A_{\rm s}$, and its spectral index, $n_{\rm s}$. CMB lensing also helps to reduce the degeneracy with $A_{\rm s}$, while getting rid of the tension with the phenomenological lensing parameter $A_{\rm L}$ when using PlanckTT only (see Planck Collaboration XIII 2016), even if the impact on the error bars is small. Comparing the posteriors in Fig. 6 with the constraints from PlanckTT alone (see Fig. 45 in Planck Collaboration XI 2016) shows that indeed, the polarization likelihood is sufficiently powerful that it breaks the degeneracy between $n_{\rm s}$ and τ. The impact on other ΛCDM parameters is small, typically below 0.3σ (as shown more explicitly in Appendix B). The largest changes are for τ and $A_{\rm s}$, where the `lollipop` likelihood dominates the constraint. The parameter σ_8 shifts towards slightly smaller values by about 1σ. This is in the right direction to help resolve some of the tension with cluster abundances and weak galaxy lensing measurements, discussed in Planck Collaboration XX (2014) and Planck Collaboration XIII (2016); however, some tension still remains.

Combining with VHL data gives compatible results, with consistent error bars. The slight shift toward lower τ value (by 0.3σ) is related to the fact that the PlanckTT likelihood alone pushes towards higher τ values (see Planck Collaboration XIII 2016), while the addition of VHL data helps to some extent in reducing the tension on τ between high-ℓ and low-ℓ polarization.

As mentioned earlier, astrophysics constraints from measurements of the Gunn-Peterson effect provide strong evidence that the IGM was highly ionized by a redshift of $z \simeq 6$. This places a lower limit on the optical depth (using Eq. (1)), which in the case of instantaneous reionization in the standard ΛCDM cosmology corresponds to $\tau = 0.038$.

[6] In this case only, other ΛCDM parameters are held fixed, including $A_{\rm s} \exp(-2\tau)$.

4.2. Kinetic Sunyaev-Zeldovich effect

The Thomson scattering of CMB photons off ionized electrons induces secondary anisotropies at different stages of the reionization process. In particular, we are interested here in the effect of photons scattering off electrons moving with bulk velocity, which is called the "kinetic Sunyaev Zeldovich" or kSZ effect. It is common to distinguish between the "homogeneous" kSZ effect, arising when the reionization is complete (e.g., Ostriker & Vishniac 1986), and "patchy" (or inhomogeneous) reionization (e.g., Aghanim et al. 1996), which arises during the process of reionization, from the proper motion of ionized bubbles around emitting sources. These two components can be described by their power spectra, which can be computed analytically or derived from numerical simulations. In Planck Collaboration XI (2016), we used a kSZ template based on homogeneous simulations, as described in Trac et al. (2011).

In the following, we assume that the kSZ power spectrum is given by

$$\mathcal{D}_\ell^{\rm kSZ} = \mathcal{D}_\ell^{\rm h-kSZ} + \mathcal{D}_\ell^{\rm p-kSZ}, \tag{8}$$

where $\mathcal{D}_\ell = \ell(\ell+1)C_\ell/2\pi$ and the superscripts "h-kSZ" and "p-kSZ" stand for "homogeneous" and "patchy" reionization, respectively. For the homogeneous reionization, we use the kSZ template power spectrum given by Shaw et al. (2012) calibrated with a simulation that includes the effects of cooling and star-formation (which we label "CSF"). For the patchy reionization kSZ effect we use the fiducial model of Battaglia et al. (2013).

In the range $\ell = 1000$–7000, the shape of the kSZ power spectrum is relatively flat and does not vary much with the detailed reionization history. The relative contributions (specifically "CSF" and "patchy") to the kSZ power spectrum are shown in Fig. 7 and compared to the "homogeneous" template used in Planck Collaboration XI (2016), rescaled to unity at $\ell = 3000$.

The kSZ power spectrum amplitude does depend on the cosmological parameters (Shaw et al. 2012; Zahn et al. 2012). To deal with this, we adopt the scalings from Shaw et al. (2012),

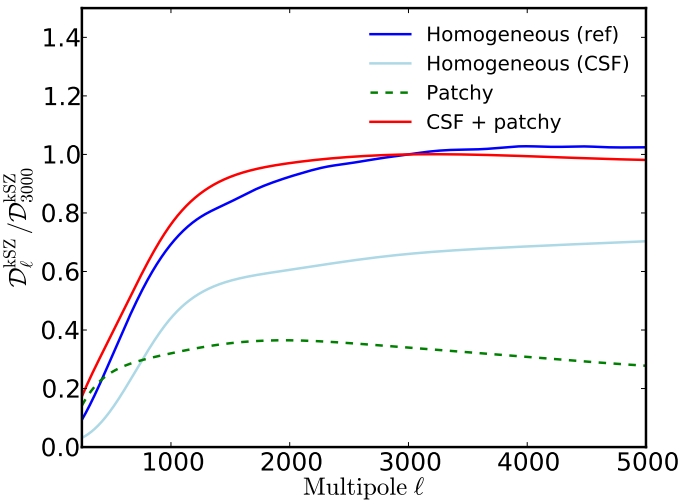

Fig. 7. Power spectrum templates for the kSZ effect. The different lines correspond to: homogeneous reionization as used in Planck Collaboration XI (2016; dark blue), based on Trac et al. (2011); "CSF" (light blue), which is a homogeneous reionization model from Shaw et al. (2012); Patchy (green dashed) based on patchy reionization model from Battaglia et al. (2013); and the sum of CSF and patchy (red).

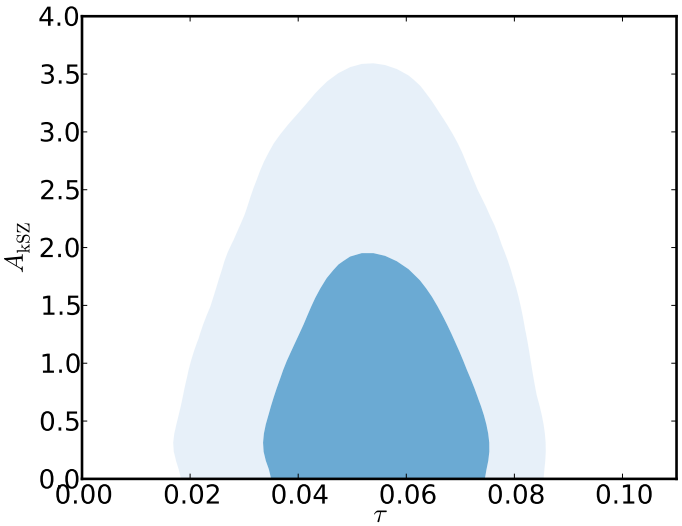

Fig. 8. 68% and 95% confidence intervals on the reionization optical depth, τ, and the amplitude of the kinetic SZ effect, $A_{\rm kSZ}$, from the CMB (`lollipop`+PlanckTT+VHL).

which gives the amplitude at $\ell = 3000$, $A_{\rm kSZ} \equiv \mathcal{D}^{\rm kSZ}_{\ell=3000}$:

$$A_{\rm kSZ} \propto \left(\frac{h}{0.7}\right)^{1.7} \left(\frac{\sigma_8}{0.8}\right)^{4.5} \left(\frac{\Omega_{\rm b}}{0.045}\right)^{2.1} \left(\frac{0.27}{\Omega_{\rm m}}\right)^{0.44} \left(\frac{0.96}{n_{\rm s}}\right)^{0.19}. \quad (9)$$

The amplitude of the kSZ power spectrum at $\ell = 3000$ for the fiducial cosmology, $A_{\rm kSZ}$ is another observable of the reionization history that can be probed by CMB data. Its scalings with the reionization redshift and the duration of the EoR can be extracted from simulations. We assume for the patchy and homogeneous kSZ effect, the scalings of Battaglia et al. (2013) and Shaw et al. (2012), respectively. For the *Planck* base ΛCDM cosmology given in Sect. 2.2, we find (in μK^2):

$$A^{\rm h}_{\rm kSZ} = 2.02 \times \left(\frac{\tau}{0.076}\right)^{0.44}; \quad (10)$$

$$A^{\rm p}_{\rm kSZ} = 2.03 \times \left[\left(\frac{1+z_{\rm re}}{11}\right) - 0.12\right] \left(\frac{z_{25\%} - z_{75\%}}{1.05}\right)^{0.51}. \quad (11)$$

For the measured value $\tau = 0.058 \pm 0.012$, Eqs. (10) and (11) give amplitudes for the homogeneous and patchy reionization contributions of $A^{\rm h}_{\rm kSZ} = 1.79\,\mu$K^2 and $A^{\rm p}_{\rm kSZ} = 1.01\,\mu$K^2, respectively.

For the multipole range of *Planck*, the amplitude of the kSZ spectrum is dominated by other foregrounds, including Galactic dust, point sources, CIB fluctuations, and the tSZ effect. Moreover, the *Planck* signal-to-noise ratio decreases rapidly above $\ell = 2000$, where the kSZ signal is maximal. This is why we cannot constrain the kSZ amplitude using *Planck* data alone. Combining with additional data at higher multipoles helps to disentangle the different foregrounds. We explicitly use the band powers from SPT (George et al. 2015) and ACT (Das et al. 2014), covering the multipole range up to $\ell = 13\,000$.

Despite our best efforts to account for the details, the kSZ amplitude is weak and there are large uncertainties in the models (both homogeneous and patchy). Moreover, there are correlations between the different foreground components, coming both from the astrophysics (we use the same halo model to derive the power spectra for the CIB and for CIB×tSZ as the one used for the kSZ effect) and from the adjustments in the data. We carried out several tests to check the robustness of the constraints on $A_{\rm kSZ}$ with respect to the template used for the CIB, CIB×tSZ, and kSZ contributions. In particular, the CIB×tSZ power spectrum amplitude is strongly anti-correlated with the kSZ amplitude and poorly constrained by the CMB data. As a consequence, if we neglect the CIB×tSZ contribution, the kSZ amplitude measured in CMB data is substantially reduced, leading to an upper limit much lower than the one derived when including the CIB×tSZ correlation. In the following discussion we consider only the more realistic case (and thus more conservative in terms of constraints on $A_{\rm kSZ}$) where the CIB×tSZ correlation contributes to the high-ℓ signal.

We combine the *Planck* likelihoods in *TT* (PlanckTT) and from low-ℓ *EE* polarization (`lollipop`) with the very high-ℓ data from ACT and SPT (VHL), assuming a redshift-symmetric parameterization of the reionization. Figure 8 shows the 2D posterior distribution for τ and $A_{\rm kSZ}$ after marginalization over the other cosmological and nuisance parameters.

Figure 9 compares the constraints on the kSZ power at $\ell = 3000$, $A_{\rm kSZ}$, obtained for three different kSZ templates: the "homogeneous" reionization template from Trac et al. (2011), which neglects contributions from inhomogeneous reionization; a more complex model "CSF & patchy," including both homogeneous and patchy contributions; and a pure "patchy" template from Battaglia et al. (2013). We find very similar upper limits on $A_{\rm kSZ}$, even in the case of pure patchy reionization.

Using the "CSF & patchy" model, the upper limit is

$$A_{\rm kSZ} < 2.6\,\mu{\rm K}^2 \quad (95\%\ {\rm CL}). \quad (12)$$

Compared to *Planck* 2013 results, the maximum likelihood value $A_{\rm kSZ} = 5.3^{+2.8}_{-1.9}\,\mu$K^2 (PlanckTT+WP+highL, Planck Collaboration XVI 2014) is reduced to an upper limit in this new analysis. The data presented here provide the best constraint to date on the kSZ power and is a factor of 2 lower than the limit reported in George et al. (2015). Our limit is certainly not in tension with the homogeneous kSZ template, which predicts $A_{\rm kSZ} = 1.79\,\mu$K^2. However, it does not leave much room for any additional kSZ power coming from patchy reionization.

Consistent with George et al. (2015), we find the total kSZ power to be stable against varying tSZ and CIB templates. We

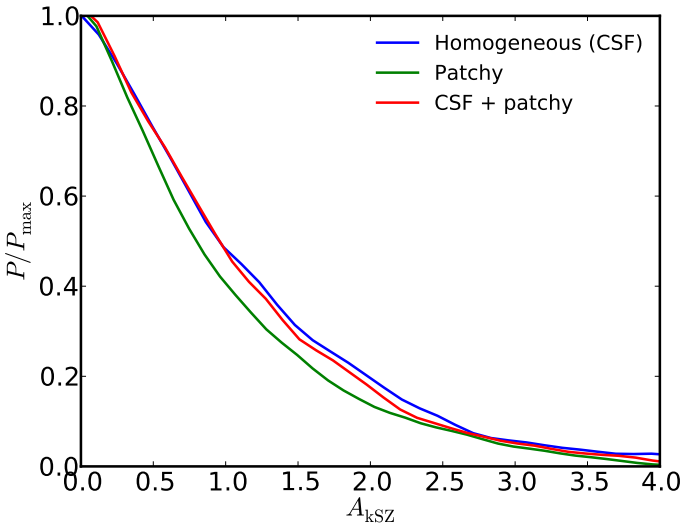

Fig. 9. Constraints on the kSZ amplitude at $\ell = 3000$ using `lollipop`+PlanckTT+VHL likelihoods. The three cases correspond to different kSZ templates.

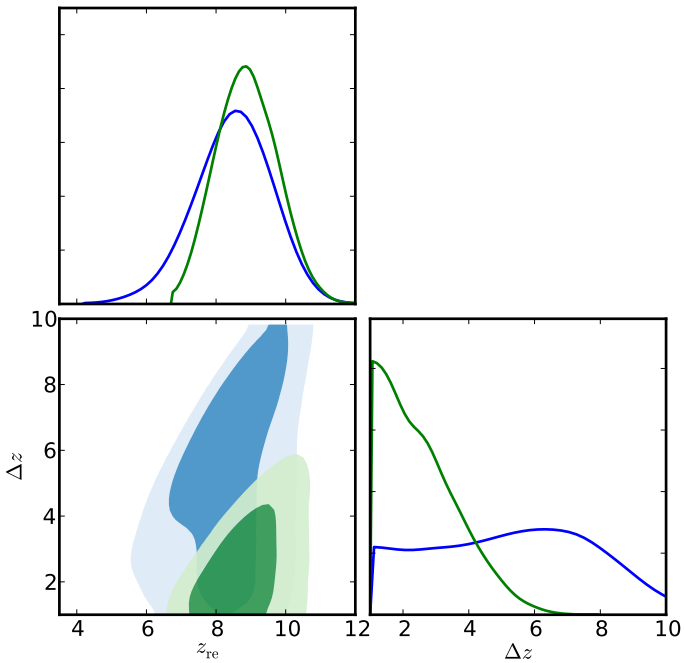

Fig. 10. Posterior distributions (in blue) of $z_{\rm re}$ and Δz for a redshift-symmetric parameterization using the CMB likelihoods in polarization and temperature (`lollipop`+PlanckTT). The green contours and lines show the distribution after imposing the additional prior $z_{\rm end} > 6$.

also find very little dependence on the choice of the kSZ template (Fig. 9). This confirms that there is only a modest amount of information in the angular shape of the kSZ signal with the current data.

5. Constraints on the reionization history

We now interpret our measurements of the reionization observables in terms of constraint on the reionization history. We mainly focus on the determination of the reionization redshift $z_{\rm re}$ and its duration $\Delta z = z_{\rm beg} - z_{\rm end}$. We show only the results for Δz greater than unity, which corresponds to approximatively 90 Myr at redshift $z = 8$. We first begin by looking at constraints on the EoR for symmetric and asymmetric models using *Planck* data only (`lollipop`+PlanckTT). Then we introduce the VHL data and discuss additional constraints from the kSZ amplitude. In each case, we also derive the constraints that follow from postulating that reionization should be completed at a redshift of 6 (see Sect. 2.1), i.e., when imposing the prior $z_{\rm end} > 6$.

5.1. Redshift-symmetric parameterization

We use the *Planck* CMB likelihoods in temperature (PlanckTT) and polarization (`lollipop`) to derive constraints on ΛCDM parameters, including the reionization redshift $z_{\rm re}$ and width Δz for a redshift-symmetric parameterization. Figure 10 shows (in blue) the posterior on $z_{\rm re}$ and Δz after marginalization over the other cosmological and nuisance parameters. As discussed in Sect. 3, the large-scale polarized CMB anisotropies are almost insensitive to the width δz of the tanh function. We thus recover the degeneracy in the direction of Δz. Imposing an additional Gunn-Peterson constraint on the ionization fraction at very low redshift can break this degeneracy. This is illustrated in Fig. 10, where we show (in green) the results of the same analysis with an additional prior $z_{\rm end} > 6$. In this case, we find $\delta z < 1.3$ at 95% CL, which corresponds to a reionization duration $(z_{\rm beg} - z_{\rm end})$ of

$$\Delta z < 4.6 \quad (95\%\ \mathrm{CL}). \tag{13}$$

The posterior distribution of $z_{\rm re}$ is shown in Fig. 10 after marginalizing over Δz, with and without the additional constraint $z_{\rm end} > 6$. This suggests that the reionization process occurred at redshift

$$z_{\rm re} = 8.5^{+1.0}_{-1.1} \quad (\text{uniform prior}), \tag{14}$$

$$z_{\rm re} = 8.8^{+0.9}_{-0.9} \quad (\text{prior } z_{\rm end} > 6). \tag{15}$$

This redshift is lower than the values derived previously from WMAP-9 data, in combination with ACT and SPT (Hinshaw et al. 2013), namely $z_{\rm re} = 10.3 \pm 1.1$. It is also lower than the value $z_{\rm re} = 11.1 \pm 1.1$ derived in Planck Collaboration XVI (2014), based on *Planck* 2013 data and the WMAP-9 polarization likelihood.

Although the uncertainty is now smaller, this new reionization redshift value is entirely consistent with the *Planck* 2015 results (Planck Collaboration XIII 2016) for PlanckTT+lowP alone, $z_{\rm re} = 9.9^{+1.8}_{-1.6}$ or in combination with other data sets, $z_{\rm re} = 8.8^{+1.3}_{-1.2}$ (specifically for PlanckTT+lowP+lensing+ BAO) estimated with δz fixed to 0.5. The constraint from `lollipop`+PlanckTT when fixing δz to 0.5 is $z_{\rm re} = 8.2^{+1.0}_{-1.2}$. This slightly lower value (compared to the one obtained when letting the reionization width be free) is explained by the shape of the degeneracy surface. Allowing for larger duration when keeping the same value of τ pushes towards higher reionization redshifts; marginalizing over Δz thus shifts the posterior distribution to slightly larger $z_{\rm re}$ values.

In addition to the posteriors for $z_{\rm re}$ and δz using the redshift-symmetric parameterization, the distributions of the end and beginning of reionization, $z_{\rm end}$ (i.e., $z_{99\%}$) and $z_{\rm beg}$ (i.e., $z_{10\%}$), are plotted in Fig. 11. In such a model, the end of reionization strongly depends on the constraint at low redshift. On the other hand, the constraints on $z_{\rm beg}$ depend only slightly on the low-redshift prior. These results show that the Universe is ionized at less than the 10% level above $z = 9.4 \pm 1.2$.

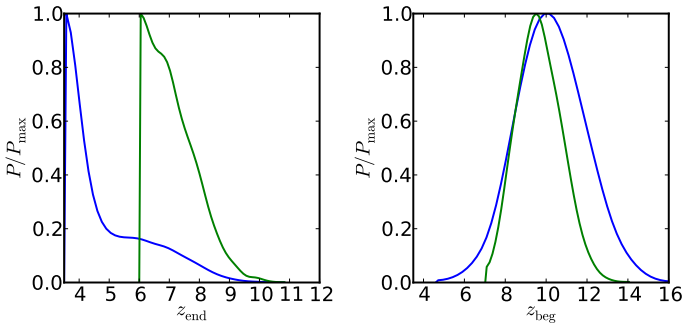

Fig. 11. Posterior distributions on the end and beginning of reionization, i.e., $z_{\rm end}$ and $z_{\rm beg}$, using the redshift-symmetric parameterization without (blue) and with (green) the prior $z_{\rm end} > 6$.

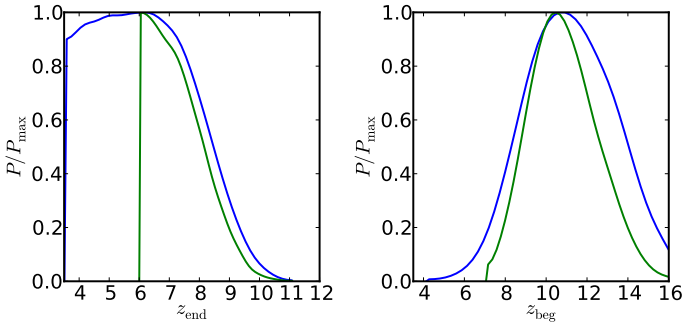

Fig. 12. Posterior distributions of $z_{\rm end}$ and $z_{\rm beg}$ using the redshift-asymmetric parameterization without (blue) and with (green) the prior $z_{\rm end} > 6$.

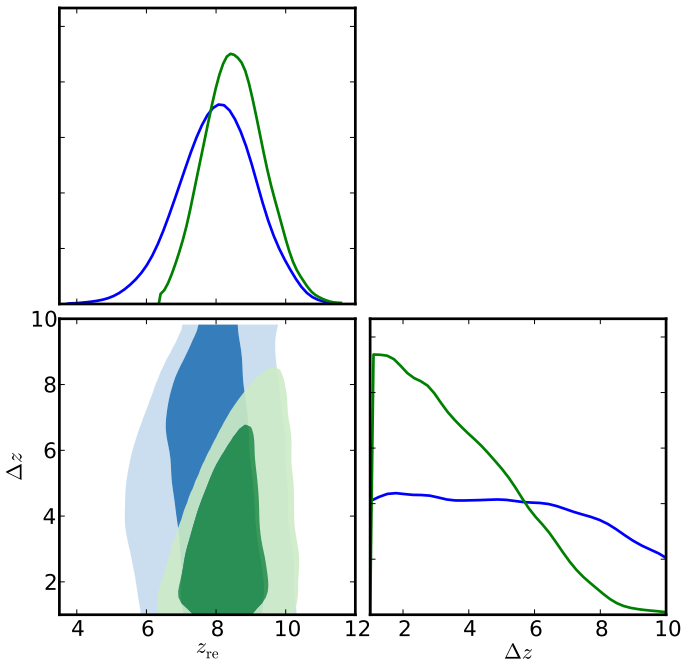

Fig. 13. Posterior distributions for $z_{\rm re}$ and Δz using the redshift-asymmetric parameterization without (blue) and with (green) the prior $z_{\rm end} > 6$.

5.2. Redshift-asymmetric parameterization

We now explore more complex reionization histories using the redshift-asymmetric parameterization of $x_{\rm e}(z)$ described in Sect. 3. In the same manner as in Sect. 5.1, also examine the effect of imposing the additional constraint from the Gunn-Peterson effect.

The distributions of the two parameters, $z_{\rm end}$ and $z_{\rm beg}$, are plotted in Fig. 12. With the redshift-asymmetric parameterization, we obtain $z_{\rm beg} = 10.4^{+1.9}_{-1.6}$ (imposing the prior on $z_{\rm end}$), which disfavours any major contribution to the ionized fraction from sources that could form as early as $z \gtrsim 15$.

In Fig. 13, we interpret the results in terms of reionization redshift and duration of the EoR, finding

$$z_{\rm re} = 8.0^{+0.9}_{-1.1} \quad \text{(uniform prior)}, \tag{16}$$

$$z_{\rm re} = 8.5^{+0.9}_{-0.9} \quad \text{(prior } z_{\rm end} > 6\text{)}. \tag{17}$$

These values are within 0.4σ of the results for the redshift-symmetric model. For the duration of the EoR, the upper limits on Δz are

$$\Delta z < 10.2 \quad \text{(95\% CL, unform prior)}, \tag{18}$$

$$\Delta z < 6.8 \quad \text{(95\% CL, prior } z_{\rm end} > 6\text{)}. \tag{19}$$

5.3. Combination with the kSZ effect

In order to try to obtain better constraints on the reionization width, we now make use of the additional information coming from the amplitude of the kinetic SZ effect. Since *Planck* alone is not able to provide accurate limits on the kSZ amplitude, we combine the *Planck* likelihoods in temperature and polarization with the measurements of the CMB TT power spectrum at high-resolution from the ACT and SPT experiments, "VHL."

Using the redshift-symmetric model, when adding the VHL data, we recover essentially the same results as in Sect. 5.1. The reionization redshift is slightly lower, as suggested by the results on τ (see Eq. (7) and the discussion in Sect. 4.1). We also see the same degeneracy along the Δz direction.

With the addition of kSZ information, we are able to break the degeneracy with Δz. This might allow us to determine how much kSZ power originated during reionization (i.e., patchy kSZ) and how much at later times, when the Universe became fully ionized (i.e., homogeneous kSZ). We use the templates from Shaw et al. (2012) and Battaglia et al. (2013) for the homogeneous and patchy kSZ contributions, respectively, with the dependency on ΛCDM cosmological parameters as described in Sect. 4.2. Those specific relations rely on a redshift-symmetric model for the description of the EoR. Note, however, that the results presented here are derived from specific simulations of the reionization process, and so explicit scalings need to be assumed, as discussed by Zahn et al. (2012) and George et al. (2015).

As described in Sect. 4.2, the amplitude of the kSZ power primarily depends on the duration of reionization, while the epoch is essentially constrained by the optical depth. Using the 2D distribution for τ and $A_{\rm kSZ}$, as measured by *Planck* in combination with very high-ℓ temperature data (Fig. 8), we derive a 2D likelihood function for $z_{\rm re}$ and Δz. We can then sample the reionization parameters (the epoch $z_{\rm re}$ and duration Δz of the EoR), compute the associated optical depth and kSZ power and derive constraints based on the 2D likelihood. The allowed models in terms of $z_{\rm re}$ and Δz are shown in Fig. 14 (in blue). We also plot (in green) the same constraints with the additional prior $z_{\rm end} > 6$.

As discussed in Sect. 4.2, the measurement of the total kSZ power constrains the amplitude of patchy reionization, resulting

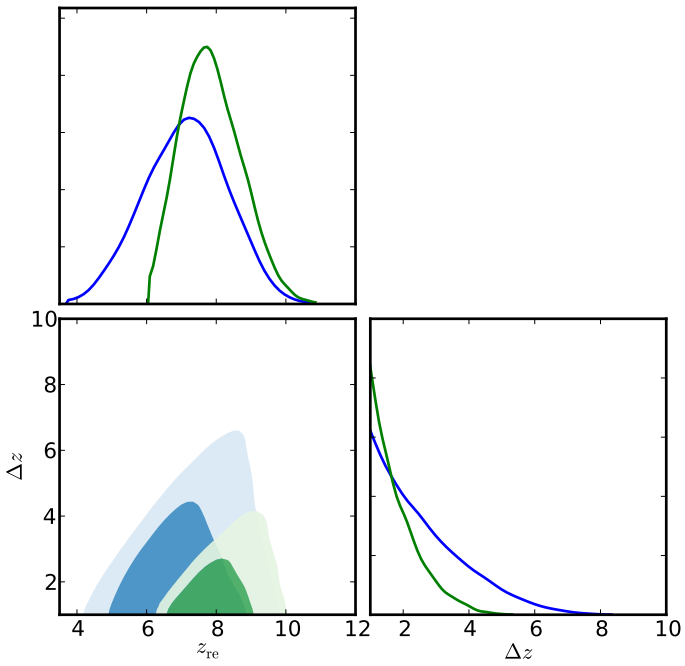

Fig. 14. Posterior distributions on the duration Δz and the redshift $z_{\rm re}$ of reionization from the combination of CMB polarization and kSZ effect constraints using the redshift-symmetric parameterization without (blue) and with (green) the prior $z_{\rm end} > 6$.

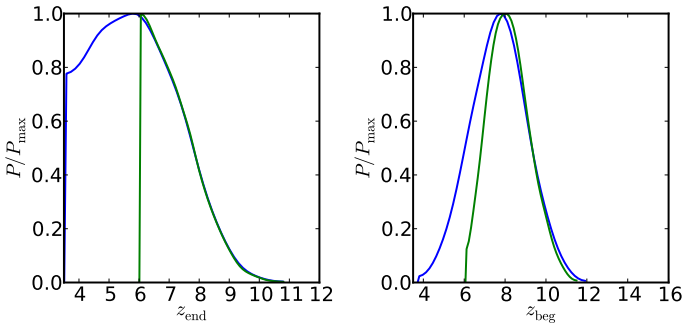

Fig. 15. Posterior distributions of $z_{\rm end}$ and $z_{\rm beg}$ using the redshift-symmetric parameterization, combining *Planck* and VHL data, and using information from the kSZ amplitude, without (blue) and with (green) the prior $z_{\rm end} > 6$.

in an upper limit of

$$\Delta z < 4.8 \quad (95\%\ \text{CL, uniform prior}), \tag{20}$$

$$\Delta z < 2.8 \quad (95\%\ \text{CL, prior } z_{\rm end} > 6). \tag{21}$$

This is compatible with the constraints from George et al. (2015), where an upper limit was quoted of $z_{20\%} - z_{99\%} < 5.4$ at 95% CL. Our 95% CL upper limits on this same quantity are 4.3 and 2.5 without and with the prior on $z_{\rm end}$, respectively.

For the reionization redshift, we find

$$z_{\rm re} = 7.2^{+1.2}_{-1.2} \quad (\text{uniform prior}), \tag{22}$$

$$z_{\rm re} = 7.8^{+1.0}_{-0.8} \quad (\text{prior } z_{\rm end} > 6), \tag{23}$$

which is compatible within 1σ with the results from CMB *Planck* data alone without the kSZ constraint (Sect. 5.1).

The distributions of $z_{\rm end}$ and $z_{\rm beg}$ are plotted in Fig. 15. Within the redshift-symmetric parameterization, we obtain $z_{\rm beg} = 8.1^{+1.1}_{-0.9}$ (with the prior on $z_{\rm end}$).

Adding information from the kSZ amplitude allows for somewhat tighter constraints to be placed on the reionization duration Δz and the beginning of reionization (corresponding to the 10% ionization limit) $z_{\rm beg}$. However, as discussed in Sect. 4.2, those results are very sensitive to details of the simulations used to predict both the shape and the parameter dependences of the kSZ template in the different reionization scenarios (patchy or homogeneous).

6. Discussion

The CMB has long held the promise of measuring the Thomson optical depth in order to derive constraints on the reionization history of the Universe. Despite its importance, this constraint is fundamentally limited by cosmic variance in polarization and is further challenged by foregrounds and systematic effects. The first results, from WMAP, gave $\tau = 0.17 \pm 0.04$, suggesting a reionization redshift between 11 and 30 (Kogut et al. 2003). This was revised in the final 9-yr WMAP results to a central value of $\tau = 0.084$ (Hinshaw et al. 2013), which, in the instantaneous reionization model, implies $z_{\rm re} = 10.4$. However, with the context of the same model, the *Planck* 2015 results (Planck Collaboration XIII 2016), either alone ($z_{\rm re} = 9.9^{+1.8}_{-1.6}$) or in combination with other data sets ($z_{\rm re} = 8.8^{+1.3}_{-1.2}$), showed that the reionization redshift was smaller. The main result we present here, $z_{\rm re} = 8.2^{+1.0}_{-1.2}$, further confirms that reionization occurred rather late, leaving little room for any significant ionization at $z \gtrsim 15$. This is consistent with what is suggested by other reionization probes, which we now discuss (for reviews, see e.g., Becker et al. 2015; McQuinn 2016).

The transition from neutral to ionized gas is constrained by absorption spectra of very distant quasars and gamma ray bursts (GRBs), revealing neutral hydrogen in intergalactic clouds. They show, through the Gunn-Peterson effect, that the diffuse gas in the Universe is mostly ionized up to a redshift of about 6 (Fan et al. 2006a). Given the decline in their abundance beyond redshift $z \simeq 6$, quasars and other active galactic nuclei (AGN) cannot be major contributors to the early stages of reionization (e.g., Willott et al. 2010; Fontanot et al. 2012, but see Madau & Haardt 2015; Khaire et al. 2016, for alternative AGN-only models). A faint AGN population can produce significant photoionization rates at redshifts of 4–6.5, consistent with the observed highly ionized IGM in the Ly-α forest of high-z quasar spectra (Giallongo et al. 2015). Star-forming galaxies at redshifts $z \gtrsim 6$ have therefore been postulated to be the most likely sources of early reionization, and their time-dependent abundance and spectral properties are crucial ingredients for understanding how intergalactic hydrogen ceased to be neutral (for reviews, see Barkana & Loeb 2001; Fan et al. 2006a; Robertson et al. 2010; McQuinn 2016). The luminosity function of early star-forming galaxies, in particular in the UV domain, is thus an additional and powerful probe of the reionization history (e.g., Kuhlen & Faucher-Giguère 2012; Robertson et al. 2013, 2015; Bouwens et al. 2015). Based on comparison of the 9-yr WMAP results to optical depth values inferred from the UV luminosity function of high-z galaxies, it has been suggested that either the UV luminosity density flattens, or physical parameters such as the escape fraction and the clumping factor evolved significantly, or alternatively, additional, undetected sources (such as X-ray binaries and faint AGN) must

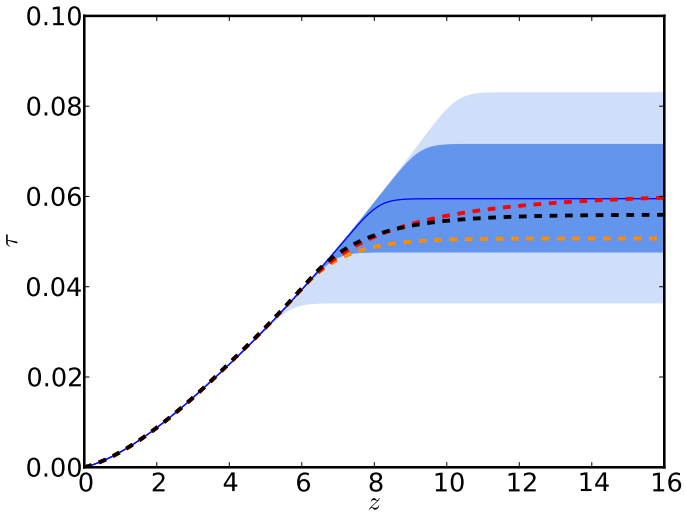

Fig. 16. Evolution of the integrated optical depth for the tanh functional form (with $\delta z = 0.5$, blue shaded area). The two envelopes mark the 68% and 95% confidence intervals. The red, black, and orange dashed lines are the models from Bouwens et al. (2015), Robertson et al. (2015), and Ishigaki et al. (2015), respectively, using high-redshift galaxy UV and IR fluxes and/or direct measurements.

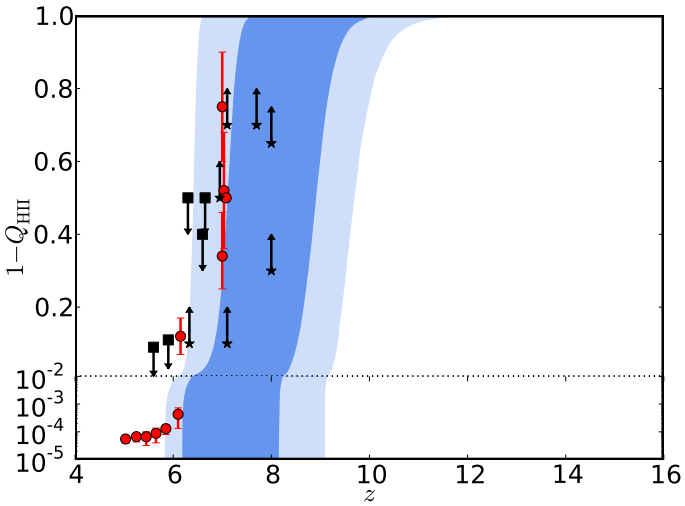

Fig. 17. Reionization history for the redshift-symmetric parameterization compared with other observational constraints coming from quasars, Ly-α emitters, and the Ly-α forest (compiled by Bouwens et al. 2015). The red points are measurements of ionized fraction, while black arrows mark upper and lower limits. The dark and light blue shaded areas show the 68% and 95% allowed intervals, respectively.

have existed at $z \gtrsim 11$ (e.g., Kuhlen & Faucher-Giguère 2012; Ellis et al. 2013; Cai et al. 2014; Ishigaki et al. 2015).

The *Planck* results, both from the 2015 data release and those presented here, strongly reduce the need for a significant contribution of Lyman continuum emission at early times. Indeed, as shown in Fig. 16, the present CMB results on the Thomson optical depth, $\tau = 0.058 \pm 0.012$, are perfectly consistent with the best models of star-formation rate densities derived from the UV and IR luminosity functions, as directly estimated from observations of high-redshift galaxies (Ishigaki et al. 2015; Robertson et al. 2015; Bouwens et al. 2015). With the present value of τ, if we maintain a UV-luminosity density at the maximum level allowed by the luminosity density constraints at redshifts $z < 9$, then the currently observed galaxy population at $M_{\rm UV} < -17$ seems to be sufficient to comply with all the observational constraints without the need for high-redshift ($z = 10$–15) galaxies.

The *Planck* data are certainly consistent with a fully reionized Universe at $z \simeq 6$. Moreover, they seem to be in good agreement with recent observational constraints on reionization in the direction of particular objects. The H I absorption along the line of sight to a distant γ-ray burst, GRB-140515A (Chornock et al. 2014), suggests a Universe containing about a 10% fraction of neutral hydrogen at $z = 6$–6.3. At even higher redshifts $z \simeq 7$, observation of Ly-α emitters suggests that at least 70% of the IGM is neutral (Tilvi et al. 2014; Schenker et al. 2014; Faisst et al. 2014). Similarly, quasar near-zone detection and analysis (including sizes, and Ly-α and β transmission properties) have been used to place constraints on $z_{\rm end}$ from signatures of the ionization state of the IGM around individual sources (Wyithe & Loeb 2004; Mesinger & Haiman 2004, 2007; Wyithe et al. 2005; Carilli et al. 2010; Mortlock et al. 2011; Schroeder et al. 2013). However, interpretation of the observed evolution of the near-zone sizes may be complicated by the opacity caused by absorption systems within the ionized IGM (e.g., Bolton et al. 2011; Bolton & Haehnelt 2013; Becker et al. 2015). Similarly, it is difficult to completely exclude the possibility that damped Ly-α systems contribute to the damping wings of quasar spectra blueward of the Ly-α line (e.g., Mesinger & Furlanetto 2008; Schroeder et al. 2013). Nevertheless, most such studies, indicate that the IGM is significantly neutral at redshifts between 6 and 7 (see also Keating et al. 2015), in agreement with the current *Planck* results, as shown in Fig. 17.

Although there are already all the constraints described above, understanding the formation of the first luminous sources in the Universe is still very much a work in progress. Our new (and lower) value of the optical depth leads to better agreement between the CMB and other astrophysical probes of reionization; however, the fundamental questions remain regarding how reionization actually proceeded.

7. Conclusions

We have derived constraints on cosmic reionization using *Planck* data. The CMB *Planck* power spectra, combining the *EE* polarization at low-ℓ with the temperature data, give, for a so-called "instantaneous" reionization history (a redshift-symmetric tanh function $x_{\rm e}(z)$ with $\delta z = 0.5$), a measurement of the Thomson optical depth

$$\tau = 0.058 \pm 0.012 \quad (\texttt{lollipop}+\text{PlanckTT}), \tag{24}$$

which is significantly more accurate than previous measurements. Thanks to the relatively high signal-to-noise ratio of the low-ℓ polarization signal, the combination with lensing or data from high-resolution CMB anisotropy experiments (ACT and SPT) does not bring much additional constraining power. The impact on other ΛCDM parameters is only significant for the amplitude of the initial scalar power spectrum $A_{\rm s}$ and (to a lesser extent) on its tilt $n_{\rm s}$. Other parameters are very stable compared to the *Planck* 2015 results.

Using *Planck* data, we have derived constraints on two models for the reionization history $x_{\rm e}(z)$ that are commonly used in

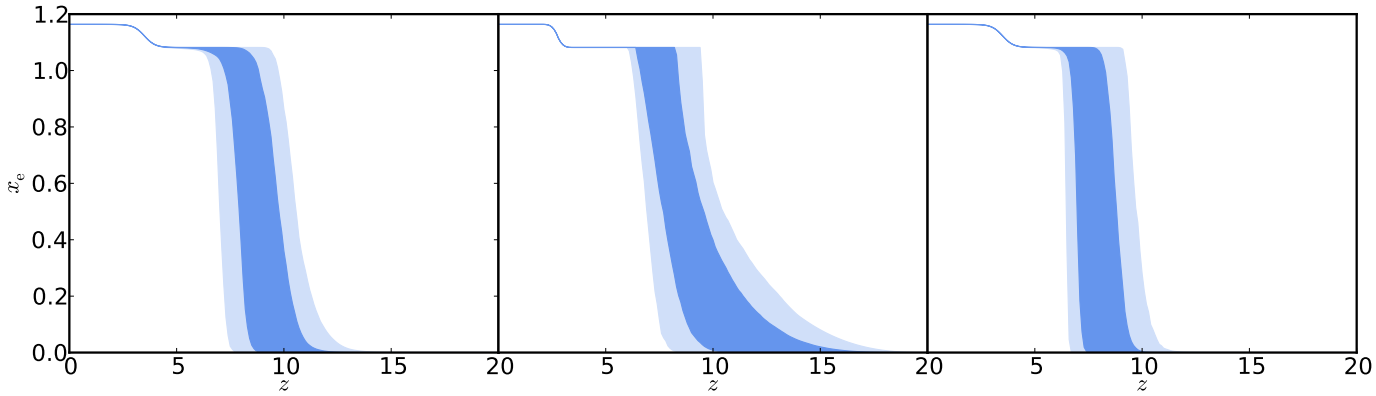

Fig. 18. Constraints on ionization fraction during reionization. The allowed models, in terms of z_{re} and Δz, translate into an allowed region in $x_e(z)$ (68% and 95% in dark blue and light blue, respectively), including the $z_{end} > 6$ prior here. *Left*: constraints from CMB data using a redshift-symmetric function ($x_e(z)$ as a hyperbolic tangent with $\delta z = 0.5$). *Centre*: constraints from CMB data using a redshift-asymmetric parameterization ($x_e(z)$ as a power law). *Right*: constraints from CMB data using a redshift-symmetric parameterization with additional constraints from the kSZ effect.

the literature: a redshift-symmetric form using a hyperbolic tangent transition function; and a redshift-asymmetric form parameterized by a power law. We have also investigated the effect of imposing the condition that the reionization is completed by $z = 6$.

Allowing the ionization fraction shape and duration to vary, we have found very compatible best-fit estimates for the optical depth (0.059 and 0.060 for the symmetric and asymmetric model, respectively), showing that the CMB is indeed more sensitive to the value of the optical depth than to the exact shape of the reionization history. However, the value of the reionization redshift does slightly depend on the model considered. In the case of a symmetric parameterization, we have found slightly larger estimates of z_{re} than in the case of instantaneous reionization. This can be understood through the shape of the degeneracy surface between the reionization parameters. For an asymmetric parameterization, z_{re} is smaller, due to the fact that $x_e(z)$ changes more rapidly at the end of reionization than the beginning. We specifically find:

$$z_{re} = 8.8 \pm 0.9 \quad \text{(redshift-symmetric)}, \tag{25}$$
$$z_{re} = 8.5 \pm 0.9 \quad \text{(redshift-asymmetric)}. \tag{26}$$

Assuming two different parameterizations of the reionization history shows how much results on effective parameters (like the redshift of reionization or its duration) are sensitive to the assumption of the reionization history shape. The best models of symmetric and asymmetric parameterization give similar values for τ, and provide reionization redshifts which differ by less than 0.4σ. Constraints on the limits of possible early reionization are similar, leading to 10% reionization levels at around $z = 10$.

To derive constraints on the duration of the reionization epoch, we combined CMB data with measurements of the amplitude of the kSZ effect. In the case of a redshift-symmetric model, we found

$$\Delta z < 2.8 \quad (95\%\ \text{CL}), \tag{27}$$

using the additional constraint that the Universe is entirely reionized at redshift 6 (i.e., $z_{end} > 6$).

Our final constraints on the reionization history are summarized on Table 1 and plotted in Fig. 18 for each of the aforementioned cases, i.e., the redshift-symmetric and redshift-asymmetric models, using only the CMB, and the redshift-symmetric case using CMB+kSZ (all with prior $z_{end} > 6$). Plotted this way, the constraints are not very tight and are still fairly model dependent. Given the low value of τ as measured now by *Planck*, the CMB is not able to give tight constraints on details of the reionization history. However, the *Planck* data suggest that an early onset of reionization is disfavoured. In particular, in all cases, we found that the Universe was less than 10% ionized for redshift $z > 10$. Furthermore, comparisons with other tracers of the ionization history show that our new result on the optical depth eliminates most of the tension between CMB-based analyses and constraints from other astrophysical data. Additional sources of reionization, non-standard early galaxies, or significantly evolving escape fractions or clumping factors, are thus not needed.

Table 1. Constraints on reionization parameters for the different models presented in this paper when including the $z_{end} > 6$ prior.

Model	z_{re}	Δz	z_{end}	z_{beg}
redshift-symmetric . .	8.8 ± 0.9	<4.6	<8.6	9.4 ± 1.2
redshift-asymmetric . .	8.5 ± 0.9	<6.8	<8.9	10.4 ± 1.8
redshift-symetrical with kSZ	7.8 ± 0.9	<2.8	<8.8	8.1 ± 1.0

Notes. We show 68% limit for z_{re} and z_{beg}, while we quote 95% upper limit for Δz and z_{end}.

Ongoing and future experiments like LOFAR, MWA, and SKA, aimed at measuring the redshifted 21-cm signal from neutral hydrogen during the EoR, should be able to probe reionization directly and measure its redshift and duration to high accuracy. Moreover, since reionization appears to happen at redshifts below 10, experiments measuring the global emission of the 21-m line over the sky (e.g., EDGES; Bowman & Rogers 2010, LEDA; Greenhill & Bernardi 2012, DARE; Burns et al. 2012, NenuFAR; Zarka et al. 2012, SARAS; Patra et al. 2013, SCI-HI; Voytek et al. 2014, ZEBRA; Mahesh et al. 2014, and BIGHORNS, Sokolowski et al. 2015) will also be able to derive very competitive constraints on the models (e.g., Liu et al. 2016; Fialkov & Loeb 2016).

Acknowledgements. The Planck Collaboration acknowledges the support of: ESA; CNES, and CNRS/INSU-IN2P3-INP (France); ASI, CNR, and INAF (Italy); NASA and DoE (USA); STFC and UKSA (UK); CSIC, MINECO, J.A., and RES (Spain); Tekes, AoF, and CSC (Finland); DLR and MPG (Germany); CSA (Canada); DTU Space (Denmark); SER/SSO (Switzerland); RCN (Norway); SFI (Ireland); FCT/MCTES (Portugal); ERC and PRACE (EU). A description of the Planck Collaboration and a list of its members, indicating which technical or scientific activities they have been involved in, can be found at http://www.cosmos.esa.int/web/planck/planck-collaboration

References

Aghanim, N., Desert, F. X., Puget, J. L., & Gispert, R. 1996, A&A, 311, 1
Aghanim, N., Majumdar, S., & Silk, J. 2008, Rep. Prog. Phys., 71, 066902
Ahn, K., Iliev, I. T., Shapiro, P. R., et al. 2012, ApJ, 756, L16
Barkana, R., & Loeb, A. 2001, Phys. Rep., 349, 125
Battaglia, N., Natarajan, A., Trac, H., Cen, R., & Loeb, A. 2013, ApJ, 776, 83
Becker, R. H., Fan, X., White, R. L., et al. 2001, AJ, 122, 2850
Becker, G. D., Bolton, J. S., Haehnelt, M. G., & Sargent, W. L. W. 2011, MNRAS, 410, 1096
Becker, G. D., Bolton, J. S., & Lidz, A. 2015, PASA, 32, e045
Bolton, J. S., & Haehnelt, M. G. 2013, MNRAS, 429, 1695
Bolton, J. S., Haehnelt, M. G., Warren, S. J., et al. 2011, MNRAS, 416, L70
Bouwens, R. J., Illingworth, G. D., Oesch, P. A., et al. 2015, ApJ, 811, 140
Bowman, J. D., & Rogers, A. E. E. 2010, Nature, 468, 796
Burns, J. O., Lazio, J., Bale, S., et al. 2012, Adv. Space Res., 49, 433
Cai, Z.-Y., Lapi, A., Bressan, A., et al. 2014, ApJ, 785, 65
Calabrese, E., Hlozek, R. A., Battaglia, N., et al. 2013, Phys. Rev. D, 87, 103012
Carilli, C. L., Wang, R., Fan, X., et al. 2010, ApJ, 714, 834
Cen, R. 2003, ApJ, 591, 12
Chornock, R., Berger, E., Fox, D. B., et al. 2014, ArXiv e-prints [arXiv:1405.7400]
Ciardi, B., Ferrara, A., & White, S. D. M. 2003, MNRAS, 344, L7
Colombo, L. P. L., & Pierpaoli, E. 2009, New Astron., 14, 269
Couchman, H. M. P., & Rees, M. J. 1986, MNRAS, 221, 53
Das, S., Louis, T., Nolta, M. R., et al. 2014, J. Cosmol. Astropart. Phys., 4, 14
Douspis, M., Aghanim, N., Ilić, S., & Langer, M. 2015, A&A, 580, L4
Dunkley, J., Komatsu, E., Nolta, M. R., et al. 2009, ApJS, 180, 306
Ellis, R. S., McLure, R. J., Dunlop, J. S., et al. 2013, ApJ, 763, L7
Faisst, A. L., Capak, P., Carollo, C. M., Scarlata, C., & Scoville, N. 2014, ApJ, 788, 87
Fan, X., Strauss, M. A., Becker, R. H., et al. 2006a, AJ, 132, 117
Fan, X., Strauss, M. A., Richards, G. T., et al. 2006b, AJ, 131, 1203
Fialkov, A., & Loeb, A. 2016, ApJ, 821, 59
Fontanot, F., Cristiani, S., & Vanzella, E. 2012, MNRAS, 425, 1413
Furlanetto, S. R., Zaldarriaga, M., & Hernquist, L. 2004, ApJ, 613, 1
George, E. M., Reichardt, C. L., Aird, K. A., et al. 2015, ApJ, 799, 177
Giallongo, E., Grazian, A., Fiore, F., et al. 2015, A&A, 578, A83
Gnedin, N. Y. 2000, ApJ, 535, 530
Greenhill, L. J., & Bernardi, G. 2012, ArXiv e-prints [arXiv:1201.1700]
Gruzinov, A., & Hu, W. 1998, ApJ, 508, 435
Gunn, J. E., & Peterson, B. A. 1965, ApJ, 142, 1633
Hamimeche, S., & Lewis, A. 2008, Phys. Rev. D, 77, 103013
Hasselfield, M., Moodley, K., Bond, J. R., et al. 2013, ApJS, 209, 17
Hinshaw, G., Larson, D., Komatsu, E., et al. 2013, ApJS, 208, 19
Holder, G. P., Haiman, Z., Kaplinghat, M., & Knox, L. 2003, ApJ, 595, 13
Hu, W., & Holder, G. P. 2003, Phys. Rev. D, 68, 023001
Iliev, I. T., Mellema, G., Ahn, K., et al. 2014, MNRAS, 439, 725
Ishigaki, M., Kawamata, R., Ouchi, M., et al. 2015, ApJ, 799, 12
Keating, L. C., Haehnelt, M. G., Cantalupo, S., & Puchwein, E. 2015, MNRAS, 454, 681
Khaire, V., Srianand, R., Choudhury, T. R., & Gaikwad, P. 2016, MNRAS, 457, 4051
Kogut, A., Spergel, D. N., Barnes, C., et al. 2003, ApJS, 148, 161
Komatsu, E., Smith, K. M., Dunkley, J., et al. 2011, ApJS, 192, 18
Kuhlen, M., & Faucher-Giguère, C.-A. 2012, MNRAS, 423, 862
Lesgourgues, J. 2011, ArXiv e-prints [arXiv:1104.2932]
Lewis, A. 2008, Phys. Rev. D, 78, 023002
Lewis, A., Weller, J., & Battye, R. 2006, MNRAS, 373, 561
Liu, A., Pritchard, J. R., Allison, R., et al. 2016, Phys. Rev. D, 93, 043013
Madau, P., & Haardt, F. 2015, ApJ, 813, L8
Madau, P., Haardt, F., & Rees, M. J. 1999, ApJ, 514, 648
Mahesh, N., Subrahmanyan, R., Udaya Shankar, N., & Raghunathan, A. 2014, ArXiv e-prints [arXiv:1406.2585]
Mangilli, A., Plaszczynski, S., & Tristram, M. 2015, MNRAS, 453, 3174
McQuinn, M. 2016, ARA&A, 54, 313
McQuinn, M., Furlanetto, S. R., Hernquist, L., Zahn, O., & Zaldarriaga, M. 2005, ApJ, 630, 643
Meiksin, A., & Madau, P. 1993, ApJ, 412, 34
Mesinger, A. 2016, Understanding the Epoch of Cosmic Reionization (Springer International Publishing), Astrophys. Space Sci. Libr., 423
Mesinger, A., & Furlanetto, S. R. 2008, MNRAS, 385, 1348
Mesinger, A., & Haiman, Z. 2004, ApJ, 611, L69
Mesinger, A., & Haiman, Z. 2007, ApJ, 660, 923
Mesinger, A., McQuinn, M., & Spergel, D. N. 2012, MNRAS, 422, 1403
Miralda-Escude, J., & Ostriker, J. P. 1990, ApJ, 350, 1
Mitra, S., Choudhury, T. R., & Ferrara, A. 2011, MNRAS, 413, 1569
Mortlock, D. J., Warren, S. J., Venemans, B. P., et al. 2011, Nature, 474, 616
Mortonson, M. J., & Hu, W. 2008, ApJ, 672, 737
Ostriker, J. P., & Vishniac, E. T. 1986, ApJ, 306, L51
Page, L., Hinshaw, G., Komatsu, E., et al. 2007, ApJS, 170, 335
Pandolfi, S., Ferrara, A., Choudhury, T. R., Melchiorri, A., & Mitra, S. 2011, Phys. Rev. D, 84, 123522
Park, H., Shapiro, P. R., Komatsu, E., et al. 2013, ApJ, 769, 93
Patra, N., Subrahmanyan, R., Raghunathan, A., & Udaya Shankar, N. 2013, Exp. Astron., 36, 319
Peebles, P. J. E. 1968, ApJ, 153, 1
Planck Collaboration XV. 2014, A&A, 571, A15
Planck Collaboration XVI. 2014, A&A, 571, A16
Planck Collaboration XX. 2014, A&A, 571, A20
Planck Collaboration II. 2016, A&A, 594, A2
Planck Collaboration VII. 2016, A&A, 594, A7
Planck Collaboration VIII. 2016, A&A, 594, A8
Planck Collaboration IX. 2016, A&A, 594, A9
Planck Collaboration X. 2016, A&A, 594, A10
Planck Collaboration XI. 2016, A&A, 594, A11
Planck Collaboration XIII. 2016, A&A, 594, A13
Planck Collaboration XV. 2016, A&A, 594, A15
Planck Collaboration Int. XLVI. 2016, A&A, 596, A107
Pritchard, J. R., Loeb, A., & Wyithe, J. S. B. 2010, MNRAS, 408, 57
Reichardt, C. L., Shaw, L., Zahn, O., et al. 2012, ApJ, 755, 70
Robertson, B. E., Ellis, R. S., Dunlop, J. S., McLure, R. J., & Stark, D. P. 2010, Nature, 468, 49
Robertson, B. E., Furlanetto, S. R., Schneider, E., et al. 2013, ApJ, 768, 71
Robertson, B. E., Ellis, R. S., Furlanetto, S. R., & Dunlop, J. S. 2015, ApJ, 802, L19
Schenker, M. A., Ellis, R. S., Konidaris, N. P., & Stark, D. P. 2014, ApJ, 795, 20
Schroeder, J., Mesinger, A., & Haiman, Z. 2013, MNRAS, 428, 3058
Seager, S., Sasselov, D. D., & Scott, D. 2000, ApJS, 128, 407
Shaw, L. D., Rudd, D. H., & Nagai, D. 2012, ApJ, 756, 15
Sokolowski, M., Tremblay, S. E., Wayth, R. B., et al. 2015, PASA, 32, 004
Sunyaev, R. A., & Zeldovich, I. B. 1980, MNRAS, 190, 413
Tilvi, V., Papovich, C., Finkelstein, S. L., et al. 2014, ApJ, 794, 5
Trac, H., Bode, P., & Ostriker, J. P. 2011, ApJ, 727, 94
Tristram, M., Macías-Pérez, J. F., Renault, C., & Santos, D. 2005, MNRAS, 358, 833
Venemans, B. P., Findlay, J. R., Sutherland, W. J., et al. 2013, ApJ, 779, 24
Voytek, T. C., Natarajan, A., García, J. M. J., Peterson, J. B., & López-Cruz, O. 2014, ApJ, 782, L9
Willott, C. J., Delorme, P., Reylé, C., et al. 2010, AJ, 139, 906
Worseck, G., Prochaska, J. X., Hennawi, J. F., & McQuinn, M. 2014, ArXiv e-prints [arXiv:1405.7405]
Wyithe, J. S. B., & Loeb, A. 2004, Nature, 432, 194
Wyithe, J. S. B., Loeb, A., & Carilli, C. 2005, ApJ, 628, 575
Zahn, O., Reichardt, C. L., Shaw, L., et al. 2012, ApJ, 756, 65
Zarka, P., Girard, J. N., Tagger, M., & Denis, L. 2012, in SF2A-2012: Proc. Annual meeting of the French Society of Astronomy and Astrophysicss, eds. S. Boissier, P. de Laverny, N. Nardetto, et al., 687
Zel'dovich, Y. B., Kurt, V. G., & Syunyaev, R. A. 1969, Sov. J. Exp. Theoret. Phys., 28, 146

[1] APC, AstroParticule et Cosmologie, Université Paris Diderot, CNRS/IN2P3, CEA/lrfu, Observatoire de Paris, Sorbonne Paris Cité, 10 rue Alice Domon et Léonie Duquet, 75205 Paris Cedex 13, France
[2] Aalto University Metsähovi Radio Observatory and Dept of Radio Science and Engineering, PO Box 13000, 00076 Aalto, Finland
[3] African Institute for Mathematical Sciences, 6−8 Melrose Road, 7945 Muizenberg, Cape Town, South Africa

[4] Agenzia Spaziale Italiana Science Data Center, via del Politecnico snc, 00133 Roma, Italy
[5] Aix-Marseille Université, CNRS, LAM (Laboratoire d'Astrophysique de Marseille) UMR 7326, 13388 Marseille, France
[6] Aix-Marseille Université, Centre de Physique Théorique, 163 avenue de Luminy, 13288 Marseille, France
[7] Astrophysics Group, Cavendish Laboratory, University of Cambridge, J J Thomson Avenue, Cambridge CB3 0HE, UK
[8] Astrophysics & Cosmology Research Unit, School of Mathematics, Statistics & Computer Science, University of KwaZulu-Natal, Westville Campus, Private Bag X54001, 4000 Durban, South Africa
[9] CITA, University of Toronto, 60 St. George St., Toronto, ON M5S 3H8, Canada
[10] CNRS, IRAP, 9 Av. colonel Roche, BP 44346, 31028 Toulouse Cedex 4, France
[11] California Institute of Technology, Pasadena, CA 91125, USA
[12] Computational Cosmology Center, Lawrence Berkeley National Laboratory, Berkeley, CA 94720, USA
[13] DTU Space, National Space Institute, Technical University of Denmark, Elektrovej 327, 2800 Kgs. Lyngby, Denmark
[14] Département de Physique Théorique, Université de Genève, 24 quai E. Ansermet, 1211 Genève 4, Switzerland
[15] Departamento de Astrofísica, Universidad de La Laguna (ULL), 38206 La Laguna, Tenerife, Spain
[16] Departamento de Física, Universidad de Oviedo, Avda. Calvo Sotelo s/n, 33003 Oviedo, Spain
[17] Department of Astrophysics/IMAPP, Radboud University Nijmegen, PO Box 9010, 6500 GL Nijmegen, The Netherlands
[18] Department of Physics & Astronomy, University of British Columbia, 6224 Agricultural Road, Vancouver, British Columbia, Canada
[19] Department of Physics and Astronomy, Dana and David Dornsife College of Letter, Arts and Sciences, University of Southern California, Los Angeles, CA 90089, USA
[20] Department of Physics and Astronomy, University College London, London WC1E 6BT, UK
[21] Department of Physics and Astronomy, University of Sussex, Brighton BN1 9QH, UK
[22] Department of Physics, Gustaf Hällströmin katu 2a, University of Helsinki, 00560 Helsinki, Finland
[23] Department of Physics, Princeton University, Princeton, NJ 08544, USA
[24] Department of Physics, University of California, Berkeley, CA 94720, USA
[25] Department of Physics, University of California, One Shields Avenue, Davis, CA 95064, USA
[26] Department of Physics, University of California, Santa Barbara, CA 93106, USA
[27] Department of Physics, University of Illinois at Urbana-Champaign, 1110 West Green Street, Urbana, IL 61801 USA
[28] Dipartimento di Fisica e Astronomia G. Galilei, Università degli Studi di Padova, via Marzolo 8, 35131 Padova, Italy
[29] Dipartimento di Fisica e Astronomia, Alma Mater Studiorum, Università degli Studi di Bologna, viale Berti Pichat 6/2, 40127 Bologna, Italy
[30] Dipartimento di Fisica e Scienze della Terra, Università di Ferrara, via Saragat 1, 44122 Ferrara, Italy
[31] Dipartimento di Fisica, Università La Sapienza, P.le A. Moro 2, 00133 Roma, Italy
[32] Dipartimento di Fisica, Università degli Studi di Milano, via Celoria, 16, 20133 Milano, Italy
[33] Dipartimento di Fisica, Università di Roma Tor Vergata, via della Ricerca Scientifica, 1, 00133 Roma, Italy
[34] Dipartimento di Matematica, Università di Roma Tor Vergata, via della Ricerca Scientifica, 1, 00133 Roma, Italy
[35] Discovery Center, Niels Bohr Institute, Copenhagen University, Blegdamsvej 17, 2100 Copenhagen, Denmark
[36] European Space Agency, ESAC, Planck Science Office, Camino bajo del Castillo, s/n, Urbanización Villafranca del Castillo, 28691 Villanueva de la Cañada, Madrid, Spain
[37] European Space Agency, ESTEC, Keplerlaan 1, 2201 AZ Noordwijk, The Netherlands
[38] Gran Sasso Science Institute, INFN, viale F. Crispi 7, 67100 L'Aquila, Italy
[39] HGSFP and University of Heidelberg, Theoretical Physics Department, Philosophenweg 16, 69120 Heidelberg, Germany
[40] Haverford College Astronomy Department, 370 Lancaster Avenue, Haverford, PA 19041, USA
[41] Helsinki Institute of Physics, Gustaf Hällströmin katu 2, University of Helsinki, 00560 Helsinki, Finland
[42] INAF–Osservatorio Astronomico di Padova, Vicolo dell'Osservatorio 5, 35131 Padova, Italy
[43] INAF–Osservatorio Astronomico di Roma, via di Frascati 33, 00040 Monte Porzio Catone, Italy
[44] INAF–Osservatorio Astronomico di Trieste, via G. B. Tiepolo 11, 34127 Trieste, Italy
[45] INAF/IASF Bologna, via Gobetti 101, 40127 Bologna, Italy
[46] INAF/IASF Milano, via E. Bassini 15, 20133 Milano, Italy
[47] INFN-CNAF, viale Berti Pichat 6/2, 40127 Bologna, Italy
[48] INFN, Sezione di Bologna, viale Berti Pichat 6/2, 40127 Bologna, Italy
[49] INFN, Sezione di Ferrara, via Saragat 1, 44122 Ferrara, Italy
[50] INFN, Sezione di Roma 1, Università di Roma Sapienza, P.le Aldo Moro 2, 00185 Roma, Italy
[51] INFN, Sezione di Roma 2, Università di Roma Tor Vergata, via della Ricerca Scientifica, 1, 00185 Roma, Italy
[52] Imperial College London, Astrophysics group, Blackett Laboratory, Prince Consort Road, London, SW7 2AZ, UK
[53] Institut d'Astrophysique Spatiale, CNRS, Univ. Paris-Sud, Université Paris-Saclay, Bât. 121, 91405 Orsay Cedex, France
[54] Institut d'Astrophysique de Paris, CNRS (UMR 7095), 98bis boulevard Arago, 75014 Paris, France
[55] Institute of Astronomy, University of Cambridge, Madingley Road, Cambridge CB3 0HA, UK
[56] Institute of Theoretical Astrophysics, University of Oslo, Blindern, 0371 Oslo, Norway
[57] Instituto de Astrofísica de Canarias, C/Vía Láctea s/n, La Laguna, 38205 Tenerife, Spain
[58] Instituto de Física de Cantabria (CSIC-Universidad de Cantabria), Avda. de los Castros s/n, 39005 Santander, Spain
[59] Istituto Nazionale di Fisica Nucleare, Sezione di Padova, via Marzolo 8, 35131 Padova, Italy
[60] Jet Propulsion Laboratory, California Institute of Technology, 4800 Oak Grove Drive, Pasadena, CA 91109, USA
[61] Jodrell Bank Centre for Astrophysics, Alan Turing Building, School of Physics and Astronomy, The University of Manchester, Oxford Road, Manchester, M13 9PL, UK
[62] Kavli Institute for Cosmological Physics, University of Chicago, Chicago, IL 60637, USA
[63] Kavli Institute for Cosmology Cambridge, Madingley Road, Cambridge, CB3 0HA, UK
[64] LAL, Université Paris-Sud, CNRS/IN2P3, 91405 Orsay, France
[65] LERMA, CNRS, Observatoire de Paris, 61 avenue de l'Observatoire, 75000 Paris, France
[66] Laboratoire Traitement et Communication de l'Information, CNRS (UMR 5141) and Télécom ParisTech, 46 rue Barrault, 75634 Paris Cedex 13, France
[67] Laboratoire de Physique Subatomique et Cosmologie, Université Grenoble-Alpes, CNRS/IN2P3, 53 rue des Martyrs, 38026 Grenoble Cedex, France
[68] Laboratoire de Physique Théorique, Université Paris-Sud 11 & CNRS, Bâtiment 210, 91405 Orsay, France
[69] Lawrence Berkeley National Laboratory, Berkeley, California, USA
[70] Max-Planck-Institut für Astrophysik, Karl-Schwarzschild-Str. 1, 85741 Garching, Germany

[71] Mullard Space Science Laboratory, University College London, Surrey RH5 6NT, UK
[72] Nicolaus Copernicus Astronomical Center, Bartycka 18, 00-716 Warsaw, Poland
[73] Niels Bohr Institute, Copenhagen University, Blegdamsvej 17, 1165 Copenhagen, Denmark
[74] Nordita (Nordic Institute for Theoretical Physics), Roslagstullsbacken 23, 106 91 Stockholm, Sweden
[75] SISSA, Astrophysics Sector, via Bonomea 265, 34136 Trieste, Italy
[76] School of Chemistry and Physics, University of KwaZulu-Natal, Westville Campus, Private Bag X54001, 4000 Durban, South Africa
[77] School of Physics and Astronomy, University of Nottingham, Nottingham NG7 2RD, UK
[78] Simon Fraser University, Department of Physics, 8888 University Drive, Burnaby BC, Canada
[79] Sorbonne Université-UPMC, UMR 7095, Institut d'Astrophysique de Paris, 98bis boulevard Arago, 75014 Paris, France
[80] Space Research Institute (IKI), Russian Academy of Sciences, Profsoyuznaya Str, 84/32, 117997 Moscow, Russia
[81] Space Sciences Laboratory, University of California, Berkeley, CA 94720, USA
[82] Sub-Department of Astrophysics, University of Oxford, Keble Road, Oxford OX1 3RH, UK
[83] The Oskar Klein Centre for Cosmoparticle Physics, Department of Physics, Stockholm University, AlbaNova, 106 91 Stockholm, Sweden
[84] UPMC Univ. Paris 06, UMR 7095, 98bis boulevard Arago, 75014 Paris, France
[85] Université de Toulouse, UPS-OMP, IRAP, 31028 Toulouse Cedex 4, France
[86] University of Granada, Departamento de Física Teórica y del Cosmos, Facultad de Ciencias, 18010 Granada, Spain
[87] Warsaw University Observatory, Aleje Ujazdowskie 4, 00-478 Warszawa, Poland

Appendix A: the Lollipop likelihood

`lollipop`, the LOw-ℓ LIkelihood on POlarized Power-spectra, is a likelihood function based on cross-power spectra for the low multipoles. The idea behind this approach is that the noise can be considered as uncorrelated between maps and that systematics will be considerably reduced in cross-correlation compared to auto-correlation.

At low multipoles and for incomplete sky coverage, the C_ℓs are not Gaussian distributed and are correlated between multipoles. `lollipop` uses the approximation presented in Hamimeche & Lewis (2008), modified as described in Mangilli et al. (2015) to apply to cross-power spectra. The idea is to apply a change of variable $C_\ell \rightarrow X_\ell$ so that the new variable X_ℓ is Gaussian. Similarly to Hamimeche & Lewis (2008), we define

$$X_\ell = \sqrt{C_\ell^{\rm f} + O_\ell}\, g\left(\frac{\widetilde{C}_\ell + O_\ell}{C_\ell + O_\ell}\right) \sqrt{C_\ell^{\rm f} + O_\ell}, \tag{A.1}$$

where $g(x) = \sqrt{2(x - \ln(x) - 1)}$, $\widetilde{C}_\ell$ are the measured cross-power spectra, C_ℓ are the power-spectra of the model to evaluate, $C_\ell^{\rm f}$ is a fiducial model, and O_ℓ are the offsets needed in the case of cross-spectra. For multi-dimensional CMB modes (i.e., T, E, and B), C_ℓ is a 3×3 matrix of power-spectra:

$$C_\ell = \begin{pmatrix} C^{TT} & C^{TE} & C^{TB} \\ C^{ET} & C^{EE} & C^{EB} \\ C^{BT} & C^{BE} & C^{BB} \end{pmatrix}_\ell, \tag{A.2}$$

and the g function is applied to the eigenvalues of $C_\ell^{-1/2}\widetilde{C}_\ell C_\ell^{-1/2}$.

In the case of auto-spectra, the offsets are replaced by the noise bias effectively present in the measured power-spectra. For cross-power spectra, the noise bias is null and here we use the effective offsets defined from the C_ℓ noise variance:

$$\Delta C_\ell \equiv \sqrt{\frac{2}{2\ell + 1}} O_\ell. \tag{A.3}$$

The distribution of the new variable X can be approximated as Gaussian, with a covariance given by the covariance of the C_ℓs. The likelihood function of the C_ℓ given the data $\widetilde{C}_\ell$ is then

$$-2 \ln P(C_\ell | \widetilde{C}_\ell) = \sum_{\ell\ell'} X_\ell^{\rm T} M_{\ell\ell'}^{-1} X_{\ell'}, \tag{A.4}$$

where the C_ℓ covariance matrix $M_{\ell\ell'}$ is estimated via Monte Carlo simulations.

In this paper, we restrict ourselves to the one-field approximation in order to derive a likelihood function based only on the EE power spectrum at very low multipoles. We use a conservative sky fraction including 50% of the sky, with a Galactic mask based on a threshold on the polarisation amplitude measured in the 353 GHz *Planck* channel, further apodized using a 4° Gaussian taper (see Fig. A.1). We use `Xpol` (a pseudo-C_ℓ estimator described in Tristram et al. 2005 extended to polarisation) to derive cross-power spectra between the 100 and 143 GHz channel maps from *Planck*. We also reject the first two multipoles ($\ell = 2$ and 3), since they are more subject to contamination by residual instrumental effects (see Planck Collaboration Int. XLVI 2016).

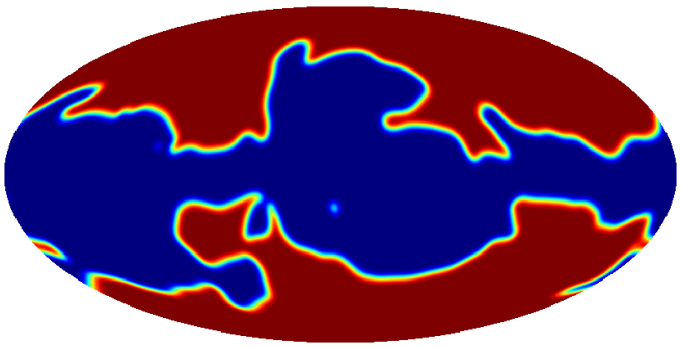

Fig. A.1. Galactic mask used for the `lollipop` likelihood, covering 50% of the sky.

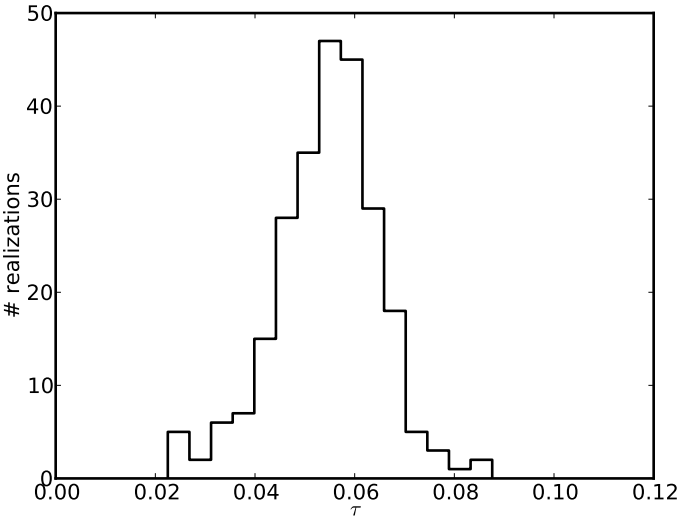

Fig. A.2. Distribution of the peak value of the posterior distribution for optical depth from end-to-end simulations including noise, systematic effects, Galactic dust signal, and CMB with the fiducial value of $\tau = 0.06$.

This likelihood has been tested on Monte Carlo simulations including signal (CMB and foregrounds), realistic noise, and systematic effects. The simulated maps are then foreground-subtracted, using the same procedure as for the data. We constructed the C_ℓ covariance matrix $M_{\ell\ell'}$ using those simulations. Figure A.2 shows the distribution of the recovered τ values for an input model with $\tau = 0.06$, fixing all other cosmological parameters to the *Planck* 2015 best-fit values (including $A_{\rm s}e^{-2\tau}$).

To validate the choice of multipole and the stability of the result on τ, we performed several consistency checks on the *Planck* data. Among them, we varied the minimum multipole used (from $\ell = 2$ to $\ell = 4$) and allowed for larger sky coverage (increasing to 60% of the sky). The results are summarized in Fig. A.3.

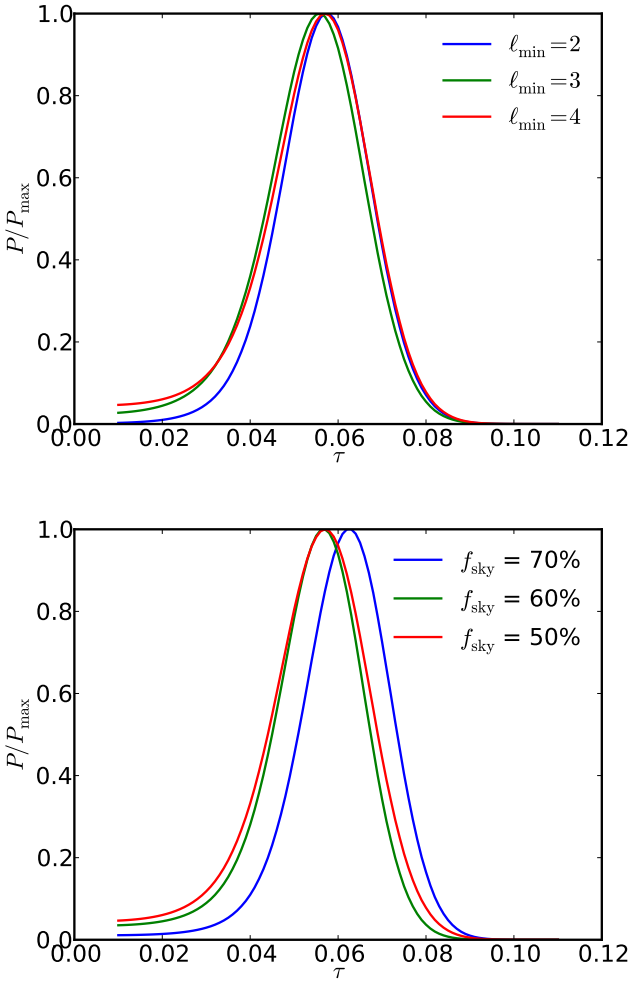

Fig. A.3. Posterior distributions for optical depth, showing the effect of changing two of the choices made in our analysis. *Top*: different choices of minimum multipole. *Bottom*: different choices of sky fraction used.

Appendix B: Impact on ΛCDM parameters

In addition to the restricted parameter set shown in Fig. 6, we describe here the impact of the `lollipop` likelihood on ΛCDM parameters in general. Figure B.1 compares results from `lollipop`+PlanckTT with the lowP+PlanckTT 2015. The new low-ℓ polarization results are sufficiently powerful that they break the degeneracy between $n_{\rm s}$ and τ. The contours for τ and $A_{\rm s}$, where the `lollipop` likelihood dominates the constraint, are significantly reduced. The impact on other ΛCDM parameters are small, typically below 0.3σ.

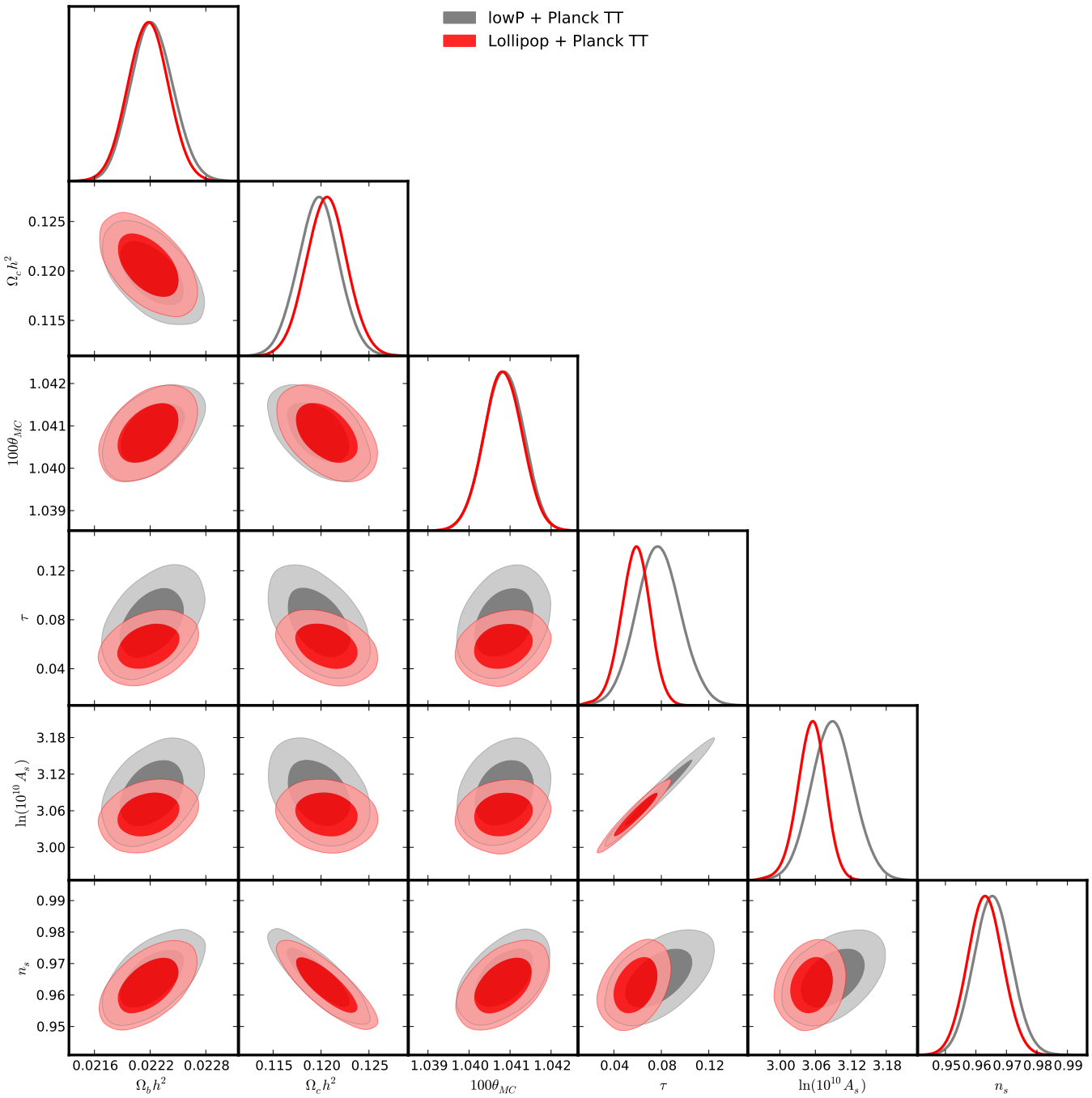

Fig. B.1. ΛCDM parameters for PlanckTT combined with the low-ℓ polarization likelihood from the *Planck* 2015 release (lowP, in grey) and from this work (`lollipop`, in red).